Low-spin states in ^{118}Sn populated by the radiative capture of thermal neutrons

K. Ortner,[1] C. Andreoiu,[1] C. M. Petrache,[2] Chong Qi,[3] A. Astier,[2] T. D. Bucher,[4] G. Colombi,[5] E. Dupont,[2] F. H. Garcia,[1,*] P. E. Garrett,[6] S. Guo,[7] G. Häfner,[8] B. Jigmeddorj,[6] J. Jolie,[8] F. Kandzia,[5] V. Karayonchev,[8] Y.-H. Kim,[5] L. Knafla,[8] B. F. Lv,[2,7] N. Mărginean,[9] E. McGee,[6] C. Michelagnoli,[5] C. Mihai,[9] P. Mutti,[5] C. Porzio,[10] K. Raymond,[1] J.-M. Régis,[8] N. Saed-Samii,[8] P. Spagnoletti,[1] W. Urban,[11] S. Valbuena,[6] J. R. Vanhoy,[12] K. Whitmore,[1] J. Wisniewski,[11] and S. W. Yates[13]

[1]*Department of Chemistry, Simon Fraser University, Burnaby, British Columbia, Canada, V5A 1S6*
[2]*University Paris-Saclay, CNRS/IN2P3, IJCLab, 40591 Orsay, France*
[3]*Department of Physics, Royal Institute of Technology (KTH), SE-10691, Stockholm, Sweden*
[4]*iThemba LABS, National Research Foundation, P.O. Box 722, 7129 Somerset West, South Africa*
[5]*Institut Laue-Langevin, 71 Avenue des Martyrs, F-38042 Grenoble, France*
[6]*Department of Physics, University of Guelph, Guelph, Ontario, Canada, NIG 2W1*
[7]*Institute of Modern Physics, Chinese Academy of Sciences, Lanzhou 730000, China*
[8]*Institut für Kernphysik, Universität zu Köln, Zülpicher Strasse 77, 50937 Köln, Germany*
[9]*Horia Hulubei National Institute for Physics and Nuclear Engineering, 77125 Bucharest, Romania*
[10]*Istituto Nazionale di Fisica Nucleare (INFN), Sezione of Milano and Dipartimento di Fisica, Università di Milano, Milano, Italy*
[11]*Faculty of Physics, University of Warsaw, ulica Pasteura 5, PL-02-093 Warsaw, Poland*
[12]*Physics Department, United States Naval Academy, Annapolis, Maryland 21402, USA*
[13]*University of Kentucky, Lexington, Kentucky 40506-0055, USA*

(Received 25 January 2024; revised 29 February 2024; accepted 2 May 2024; published 17 May 2024)

Background: γ-ray spectroscopy studies of the Sn isotopes provide important information on nuclear structure and shell evolution across the long isotopic chain between the doubly-magic ^{100}Sn and ^{132}Sn nuclei. These studies also offer great value to test and tune nuclear models which can then be applied to other regions of the nuclear chart.

Purpose: We aim to expand the level scheme of ^{118}Sn by populating low-spin states in the range of 3–5 MeV and determine their angular momentum for the possible connection of these states to pygmy quadrupole Resonances, a new phenomenon observed in the neighboring ^{112,114,124}Sn isotopes as a resonance-like structure in the 3–5 MeV range.

Method: Excited states in ^{118}Sn were populated via the ^{117}Sn$(n,\gamma)^{118}$Sn reaction at the Institut Laue-Langevin in Grenoble, France. The FIssion Product Prompt gamma-ray Spectrometer (FIPPS), an array of eight n-type high purity Germanium clover detectors augmented with eight additional clover detectors from IFIN "Horia Hulubei" were used to detect γ rays from excited states in ^{118}Sn. The array provides a superior efficiency for γ-ray detection and nearly 4π coverage for the measurements of angular correlations for spin assignment of excited nuclear levels.

Results: Through γ-γ coincidences, 112 excited states were identified with 57 being newly placed in the level scheme. From these states, 567 γ-ray transitions were observed with 501 being newly identified. Many levels were identified in the 3–5 MeV region. Further, an indirect measurement of the $E0$ transition which decays from the 0_3^+ state to the 2p-2h, 0_2^+ state was performed and the $q_K^2(E0/E2)$ and $X(E0/E2)$ for this transition were determined to be 12.7(11) and 6.3(5), respectively. The $10^3 \times \rho^2(E0)$ was determined to be >38 based on a half-life limit of <200 ps of the 2057-keV, 0_3^+ level.

Conclusions: The abundant spectroscopic information on ^{118}Sn obtained in the present experiment is an important input to the theoretical description of nuclei in the region and highlights the capabilities of the FIPPS array at ILL in conjunction with neutron capture reactions. Many states identified in the 3–5 MeV region could very likely have $J = 2^+$ and contribute to the pygmy quadrupole resonances.

DOI: 10.1103/PhysRevC.109.054317

I. INTRODUCTION

Due to the magic closed shell at proton number $Z = 50$, there exist ten stable isotopes of tin, the most for a given element. Stretching between two major closed neutron (N) shells, from the doubly-magic ^{100}Sn$_{50}$ to ^{132}Sn$_{82}$ and beyond,

*Present address: Lawrence Berkeley National Laboratory, 1 Cyclotron Rd, Berkeley, CA 94720, USA.

tin is perhaps the best example of nuclear stability. The long isotopic chain makes tin a benchmark for models of nuclear structure and many studies have been performed using an extensive variety of theoretical and experimental methods.

Theoretical studies have described the structure of the lightest tin isotopes [1] and shape evolution across the entire isotopic chain [2], as well as testing of shell model calculations using the generalized-seniority scheme [3]. The neutron-rich tin nuclei around the magic 82 neutron number play an important role in astrophysics for the understanding of the rapid-capture nuclear process [4–9]. A feature of the mid-shell tin isotopes is the presence of shape coexistence: collective excitations at low energy in the form of rotational bands built on prolate shapes arising from two-particle–two-hole (2p-2h) excitations across the $Z = 50$ shell gap [10–13].

Recently, at excitation energies near and below the particle threshold, a phenomenon called pygmy dipole resonance (PDR) was observed in mid-shell tin isotopes [14–16]. The PDR is generally described as being split into two parts, a lower-lying isoscalar surface mode attributed to neutron-skin oscillations, and a higher-lying isovector mode [17,18]. Evidence of these PDR states led to the question of a neutron-skin oscillation with a higher multipolarity, i.e., a pygmy quadrupole resonance (PQR). Excited states believed to be attributed to the PQR were recently observed in ^{112,114,124}Sn between 3 and 5 MeV as a resonance-like structure composed of 2^+ states [19,20]. In those studies, theoretical calculations (energy-density functional and three-phonon quasiparticle-phonon model theory) coupled with the experimental data hinted at a low-energy quadrupole mode occurring as a quadrupole-type oscillation of the neutron skin.

Recent thermal neutron capture, (n, γ), experiments to study PQR states in ^{116,118,120}Sn nuclei were performed at the Institut Laue-Langevin (ILL) using enriched ^{115,117,119}Sn targets. While the primary goal of the ^{115}Sn$(n, \gamma)^{116}$Sn experiment was to measure lifetimes of states belonging to the 2p-2h intruder band and to better understand the mixing of the 2p-2h band with the normal configuration [12], the intent of all three complimentary (n, γ) reactions was to populate 2^+ states in the 3–5 MeV region in each of ^{116,118,120}Sn to identify the presence of a PQR and make comparisons to the previous PQR studies on ^{112,114,124}Sn [19,20]. In this paper, the analysis of ^{117}Sn$(n, \gamma)^{118}$Sn reaction is discussed.

II. EXPERIMENT

The present experiment was performed at the Institut Laue-Langevin in Grenoble, France, with a 10^8 neutrons/(cm^2 s) beam produced by the on-site 57 MW research reactor [21]. The neutrons produced in the fission reactions inside the reactor core were moderated to thermal energies by the heavy water and were delivered via the thermal neutron guide H22 [22]. The collimated neutron beam bombarded a 300 mg, 92.8% isotopically enriched ^{117}Sn target with a thermal neutron absorption cross section of 1.32(18) b [23].

The neutron capture reaction, which ran for approximately two days, populated a quasicontinuum of states in ^{118}Sn at the neutron separation energy of 9.326 MeV [24]. Given the $J^\pi = 1/2^+$ ground state of ^{117}Sn and the $1/2^+$ S-wave thermal neutron, population of only capture states of $J^\pi = 0^+$ and 1^+ is expected. This allows for direct population of potential 2^+, PQR states via the primary γ rays.

The γ rays emitted from de exciting states in ^{118}Sn were detected with the FIssion Product Prompt gamma-ray Spectrometer (FIPPS) [22], an array of eight high purity germanium (HPGe) clover detectors that form a ring with a 9 cm radius around the target. Furthermore, eight additional HPGe clover detectors were provided by IFIN "Horia Hulubei", in Bucharest, Romania, to enhance the total efficiency and angular coverage. Each clover is composed of four HPGe crystals, which were utilized in addback mode. This technique adds the scattered events that occur within a 300 ns time window between adjacent crystals in the same clover which greatly enhanced photopeak efficiency which was determined to be over twice the efficiency of the normal singles mode at energies above 6 MeV. One clover and one crystal of the IFIN detectors, as well as two FIPPS crystals, were not included in this analysis due to poor electronic response.

The efficiency was measured by using a standard source of ^{152}Eu and a ^{27}Al$(n, \gamma)^{28}$Al reaction prior to the experiment. In the calibration process, linear gain-matching of two intense transitions with well known energies was made for each detector. The transitions used were 121 and 1408 keV from ^{152}Eu, 983 and 7724 keV from ^{27}Al$(n, \gamma)^{28}$Al, and 511 keV and the $2^+_1 \rightarrow 0^+_{\text{g.s.}}$ 1230 keV from ^{118}Sn. Furthermore, corrections for the nonlinear response of the detectors and for cross-talk were made. The cross-talk corrections were carried out as described in Ref. [25]. The total detector efficiency of FIPPS and IFIN in addback mode was 9.9(2)% at 1.3 MeV. The energy resolution, or full width at half maximum (FWHM), was 2.33 keV at 1.3 MeV and 6.9 keV at 9.3 MeV. A systematic uncertainty on the γ-ray energies was determined to be 0.3 keV. This was determined by taking the difference of the measured photopeak centroids in the calibrated spectra to the well-known γ-ray energies from ^{152}Eu, ^{118}Sn, and ^{27}Al$(n, \gamma)^{28}$Al.

The placement of γ-ray transitions to a partial level scheme was determined using a γ-γ-coincidence matrix. In total, 3×10^{10} coincident events were recorded for ^{118}Sn. Time-random background was subtracted from the prompt events to ensure only true coincidence events were analyzed. The intensities that were measured were corrected for summing effects using the 180° coincidence-method outlined in Ref. [25].

III. RESULTS

In total, 567 γ-ray transitions were placed from 112 energy levels. Of these, 501 transitions and 57 levels are newly added to the current evaluated level scheme [24]. Furthermore, 86 of these are primary transitions originating from the capture state at 9326 keV. These values are presented in Table I, where the branching ratios are compared to Ref. [10].

Only one previous (n, γ) study on ^{118}Sn, which has extensive γ-ray spectroscopy data, exists in the literature [26]. Of their findings, 162 γ-ray transitions were placed between 45 energy levels. The reported measured intensities are comparable to the present measurements and their findings suggest a capture state of predominately $J^\pi = 1^+$, which is in line

TABLE I. Observed levels and transitions from the present ^{117}Sn$(n,\gamma)^{118}$Sn experiment. Level energies were fit to the γ-ray transition energies using a least-squares fit. The energies in bold are the newly placed transitions and levels which are not in the current Evaluated Nuclear Structure Data File (ENSDF) sheet [24]. Spins of newly placed states are given based on γ decay selection rules. Branching ratios are compared to a previous high-statistics study involving β decay of the 5^+ isomer of ^{118}In [10].

$E_{\text{level},i}$ (keV)	J_i^π	$E_{\text{level},f}$ (keV)	J_f^π	E_γ (keV)	I_γ	$I_\gamma^{\text{norm.}}$	$I_\gamma^{\text{norm.}}$ [10]
1229.50(7)	2^+	0	0^+	1229.7(3)	100	100	100
1758.08(9)	0^+	1229.50	2^+	528.9(3)	6.5(2)	100	100
2042.67(8)	2^+	1758.08	0^+	284.5(3)	0.12(3)	1.1(3)	1.31(17)
		1229.50	2^+	813.3(3)	11.3(4)	100(3)	100.0(23)
		0	0^+	2042.9(3)	8.3(3)	74(3)	83.6(26)
2056.66(9)	0^+	1229.50	2^+	827.3(3)	5.26(18)	100	
2280.23(14)	4^+	1229.50	2^+	1050.7(3)	5.31(17)	100	100
2321.1(2)	5^-	2280.23	4^+	41.0(3)		100(3)	
		1229.50	2^+	1091.5(3)		8.6(9)	
2324.77(10)	3^-	1229.50	2^+	1095.2(3)	9.1(3)	100	100(5)
2327.82(9)	2^+	2042.67	2^+	285.2(3)	0.156(19)	1.69(20)	2.3(8)
		1758.08	0^+	569.6(3)	0.255(12)	2.76(13)	2.40(14)
		1229.50	2^+	1098.4(3)	9.2(3)	100(4)	100(4)
		0	0^+	2328.0(3)	1.52(8)	16.6(8)	19.1(8)
2403.01(9)	2^+	2042.67	2^+	360.4(3)	0.102(9)	1.29(12)	0.91(13)
		1758.08	0^+	644.8(3)	0.108(9)	1.36(11)	1.44(6)
		1229.50	2^+	1173.7(3)	7.9(4)	100(4)	100.0(26)
2488.57(14)	4^+	2280.23	4^+	208.6(3)	0.372(13)	47.3(16)	60.3(12)
		2042.67	2^+	446.0(3)	0.79(5)	100(6)	100.0(22)
		1229.50	2^+	1259.1(3)	0.54(9)	69(12)	59.2(16)
2496.78(12)	0^+	1229.50	2^+	1267.6(3)	2.55(11)	100	
2677.20(10)	2^+	2403.01	2^+	**274.2(3)**	0.073(5)	2.8(2)	
		2327.82	2^+	**349.4(3)**	0.063(8)	2.4(3)	
		2056.66	0^+	620.5(3)	0.016(4)	0.62(17)	
		1758.08	0^+	918.8(3)	0.108(9)	4.1(3)	
		1229.50	2^+	1447.7(3)	2.36(9)	90(5)	87(6)
		0	0^+	2677.3(3)	2.61(13)	100(5)	100(6)
2733.6(3)	4^+	1229.50	2^+	1504.1(3)	0.92(4)	100	100(3)
2737.89(10)	1^+	2327.82	2^+	**410.0(3)**	0.41(3)	9.4(6)	
		1758.08	0^+	**979.7(3)**	0.020(6)	0.46(14)	
		1229.50	2^+	1508.4(3)	4.37(16)	100(4)	
		0	0^+	2738.0(3)	1.30(11)	30(2)	
2773.92(17)	4^-	2324.77	3^-	449.1(3)	0.323(14)	42.1(18)	
		2321.1	5^-	452.8(3)	0.77(3)	100(4)	
2903.78(11)	2^+	2056.66	0^+	**846.8(3)**	0.017(7)	0.6(2)	
		2042.67	2^+	**861.0(3)**	0.125(19)	4.4(7)	
		1229.50	2^+	1674.2(3)	0.99(6)	35(2)	67(7)
		0	0^+	2903.9(3)	2.83(14)	100(5)	100(7)
2929.6(3)	0^+	2042.67	2^+	**886.9(7)**	0.095(14)	11.6(17)	
		1229.50	2^+	1700.1(3)	0.82(8)	100(9)	
2963.25(18)	4^+	2488.57	4^+	474.6(5)	0.019(9)	5(2)	5.26(16)
		2403.01	2^+	559.9(3)	0.011(5)	2.8(11)	1.97(4)
		2327.82	2^+	635.9(4)	0.026(7)	6.4(16)	2.94(7)
		2324.77	3^-	638.5(4)	0.013(4)	3.1(11)	2.72(6)
		2280.23	4^+	683.1(3)	0.406(9)	100(2)	100.0(23)
3057.15(17)	2^+	2327.82	2^+	**729.3(3)**	0.052(6)	3.7(4)	
		2324.77	3^-	**732.2(3)**	0.023(4)	1.6(3)	
		2042.67	2^+	**1014.1(3)**	0.047(9)	3.4(6)	
		1758.08	0^+	**1298.5(3)**	0.181(6)	13.0(4)	
		1229.50	2^+	1827.4(3)	0.315(3)	22.7(18)	
		0	0^+	3057.2(3)	1.39(9)	100((7)	
3089.3(4)	$(5)^+$	2280.23	4^+	809.0(3)	0.359(7)	100	

TABLE I. (*Continued.*)

$E_{\text{level},i}$ (keV)	J_i^π	$E_{\text{level},f}$ (keV)	J_f^π	E_γ (keV)	I_γ	$I_\gamma^{\text{norm.}}$	$I_\gamma^{\text{norm.}}$ [10]
3135.1(2)	$(2^+, 3^-)$	2403.01	2^+	**731.7(3)**	0.0277(12)	5.3(2)	
		2327.82	2^+	**807.1(3)**	0.191(15)	37(3)	
		2324.77	3^-	**810.1(3)**	0.049(2)	9.4(5)	
		2280.23	4^+	**854.7(3)**	0.151(4)	29.1(9)	
		2042.67	2^+	**1092.2(3)**	0.52(3)	100(6)	
		1229.50	2^+	**1905.6(3)**	0.273(14)	52(4)	
3137.35(3)	0^+	1229.50	2^+	1907.7(3)	0.52(2)	100	
3215.87(18)	(0^+)	2327.82	2^+	**888.3(3)**	0.31(2)	74(5)	
		2042.67	2^+	**1173.6(3)**	0.33(3)	78(7)	
		1229.50	2^+	**1986.7(3)**	0.42(4)	100(9)	
3228.27(14)	2^+	2677.20	2^+	**550.9(3)**	0.086(7)	7.5(6)	
		2488.57	4^+	**738.7(5)**	0.023(9)	2.0(8)	
		2403.01	2^+	**824.8(3)**	0.063(3)	5.4(2)	
		2327.82	2^+	**899.7(3)**	0.090(8)	7.8(7)	
		2324.77	3^-	**903.3(3)**	0.093(5)	8.1(4)	
		2280.23	4^+	**947.2(3)**	0.072(5)	6.2(4)	
		2056.66	0^+	**1171.7(3)**	0.18(3)	15(2)	
		2042.67	2^+	**1185.5(3)**	0.191(13)	16.6(11)	
		1229.50	2^+	**1998.1(3)**	0.82(8)	71(7)	
		0	0^+	3228.3(5)	1.15(6)	100(5)	
3251.9(2)	(3^+)	2403.01	2^+	**848.8(3)**	0.065(4)	6.4(4)	
		2327.82	2^+	**924.0(3)**	0.184(14)	18.2(13)	
		2324.77	3^-	**927.3(3)**	0.109(6)	10.8(6)	
		2042.67	2^+	1209.2(3)	0.225(15)	22.3(15)	
		1229.50	2^+	2022.3(3)	1.01(5)	100(5)	
3262.33(19)	3^+	2677.20	2^+	**585.2(4)**	0.027(6)	3.5(7)	
		2488.57	4^+	**773.5(3)**	0.017(6)	2.2(7)	
		2403.01	2^+	**859.2(3)**	0.062(4)	8.1(6)	
		2280.23	4^+	**982.06(3)**	0.15(5)	20(6)	
		2042.67	2^+	1219.6(3)	0.76(5)	100(6)	
3270.47(17)	1	2056.66	0^+	**1213.8(3)**	0.042(5)	2.2(3)	
		1758.08	0^+	**1512.3(3)**	0.079(7)	4.2(4)	
		1229.50	2^+	**2040.6(3)**	0.06(3)	3.3(14)	
		0	0^+	3270.7(3)	1.91(8)	100(4)	
3308.39(14)	2^+	2677.20	2^+	**631.3(3)**	0.026(7)	3.4(9)	
		2496.78	0^+	**811.4(3)**	0.048(5)	6.1(6)	
		2403.01	2^+	**905.3(3)**	0.138(5)	17.5(6)	
		2327.82	2^+	**980.5(3)**	0.043(7)	5.4(8)	
		2324.77	3^-	**983.8(3)**	0.138(5)	17.2(13)	
		2056.66	0^+	**1251.6(3)**	0.089(5)	11.3(6)	
		1229.50	2^+	2078.8(3)	0.79(4)	100(5)	
		0	0^+	3308.2(3)	0.197(13)	25.0(16)	
3352.9(2)	$0^{(+)}$	2327.82	2^+	**1025.1(3)**	0.110(13)	19(2)	
		2042.67	2^+	**1310.2(3)**	0.152(14)	26(3)	
		1229.50	2^+	**2123.4(3)**	0.58(8)	100(13)	
3355.59(13)	2^+	2903.78	2^+	**452.0(3)**	0.014(3)	2.4(4)	
		2737.89	1^+	**617.8(3)**	0.023(3)	3.1(4)	
		2677.20	2^+	**678.4(3)**	0.057(10)	9.8(17)	
		2496.78	0^+	**858.5(4)**	0.0100(16)	1.4(2)	
		2488.57	4^+	**867.1(3)**	0.027(11)	3.7(15)	
		2403.01	2^+	**952.5(3)**	0.124(8)	17.0(10)	
		2056.66	0^+	**1298.8(3)**	0.200(7)	27.5(9)	
		2042.67	2^+	**1312.9(3)**	0.149(14)	20(2)	
		1229.50	2^+	2126.2(3)	0.73(9)	100(13)	
		0	0^+	3355.9(3)	0.20(3)	27(4)	

TABLE I. (*Continued.*)

$E_{\text{level},i}$ (keV)	J_i^π	$E_{\text{level},f}$ (keV)	J_f^π	E_γ (keV)	I_γ	$I_\gamma^{\text{norm.}}$	$I_\gamma^{\text{norm.}}$ [10]
3375.49(12)	(1)	2737.89	1^+	**637.8(3)**	0.058(3)	8.5(5)	
		2677.20	2^+	**698.5(3)**	0.027(6)	3.9(8)	
		2488.57	4^+	**885.9(4)**	0.017(6)	2.5(8)	
		2403.01	2^+	**972.4(3)**	0.160(6)	23.4(8)	
		2327.82	2^+	**1047.8(3)**	0.68(5)	100(7)	
		2280.23	4^+	**1094.5(3)**	0.049(4)	7.1(6)	
		2056.66	0^+	**1318.8(3)**	0.158(7)	23.0(10)	
		2042.67	2^+	**1333.0(3)**	0.057(8)	8.3(12)	
		1758.08	0^+	**1617.4(3)**	0.142(5)	20.7(8)	
		1229.50	2^+	**2146.1(3)**	0.237(15)	35(2)	
3420.1(2)	3^+	2403.01	2^+	**1016.7(3)**	0.031(3)	20(2)	
		2327.82	2^+	**1092.0(3)**	0.098(7)	60(4)	
		2042.67	2^+	**1377.1(3)**	0.162(10)	100(6)	
		1229.50	2^+	**2190.7(3)**	0.078(8)	48(5)	
3426.9(2)	3^+	2403.01	2^+	**1023.7(3)**	0.088(4)	27.8(12)	
		2327.82	2^+	**1099.6(6)**	0.06(3)	6(3)	
		2324.77	3^-	**1102.2(3)**	0.075(3)	23.8(10)	
		2042.67	2^+	1384.0(3)	0.154(11)	63(5)	
		1229.50	2^+	2197.6(3)	0.32(3)	100(9)	
3450.4(3)	$3, 4, 5^-$	2963.25	4^+	**487.05(3)**	0.126(7)	100(5)	
		2488.57	4^+	**961.9(3)**	0.039(11)	31(9)	
		2403.01	2^+	**1047.2(4)**	0.013(3)	10(3)	
		2280.23	4^+	**1170.1(4)**	0.024(4)	19(3))	
3462.49(13)	(2^+)	2903.78	2^+	**558.7(3)**	0.063(3)	6.6(3)	
		2737.89	1^+	**724.6(3)**	0.056(4)	5.9(4)	
		2677.20	2^+	**785.3(4)**	0.025(6)	2.6(7)	
		2488.57	4^+	**974.1(4)**	0.027(7))	2.8(7))	
		2403.01	2^+	**1059.3(3)**	0.024(4)	2.5(4)	
		2324.77	3^-	**1137.9(3)**	0.297(9)	31.0(9)	
		2056.66	0^+	**1405.6(3)**	0.036(4)	3.8(4)	
		2042.67	2^+	1419.7(3)	0.96(6)	100(6)	
		1758.08	0^+	**1704.1(3)**	0.040(5)	4.2(5)	
		1229.50	2^+	**2232.8(3)**	0.089(4)	9.3(4)	
3528.7(3)	(2^+)	3057.15	2^+	**471.3(4)**	0.011(4)	5.3(19)	
		2737.89	1^+	**790.5(3)**	0.050(2)	23.6(12)	
		2677.20	2^+	**851.2(4)**	0.025(5)	12(2)	
		2496.78	0^+	**1031.2(3)**	0.011(2)	5.4(10)	
		2324.77	3^-	**1203.7(3)**	0.159(5)	76(3)	
		2057.77	0^+	**1471.5(3)**	0.020(2)	9.6(2)	
		2042.67	2^+	**1485.6(3)**	0.210(13)	100(6)	
		1758.08	0^+	**1770.2(3)**	0.139(7)	66(3)	
3554.1(3)	(3, 4)	2963.25	4^+	**590.9(3)**	0.025(4)	27(5)	
		2903.78	2^+	**650.3(3)**	0.009(2)	10(3)	
		2677.20	2^+	**877.1(3)**	0.025(6)	28(7)	
		2403.01	2^+	**1151.2(3)**	0.092(4)	100(4)	
3586.5(2)	(2^+)	2403.01	2^+	**1184.2(3)**	0.062(5)	67(6)	
		2327.82	2^+	**1258.7(3)**	0.074(6)	80(6)	
		2324.77	3^-	**1261.9(3)**	0.062(4)	67(4)	
		2280.23	4^+	**1306.1(3)**	0.093(6)	100(6)	
3623.5(2)	(2^+)	2677.20	2^+	**946.1(4)**	0.024(6)	11(2)	
		2403.01	2^+	**1220.6(7)**	0.042(14)	18(6)	
		2042.67	2^+	**1580.6(3)**	0.230(14)	100(6)	
3636.49(18)	$(1^-, 2^+)$	2737.89	1^+	**898.4(3)**	0.024(3)	5.7(7)	
		2677.20	2^+	**959.0(3)**	0.041(6)	9.5(15)	
		2327.82	2^+	**1308.3(3)**	0.069(8)	16.0(18)	
		2324.77	3^-	**1311.7(3)**	0.251(8)	59(2)	

TABLE I. (*Continued.*)

$E_{\text{level},i}$ (keV)	J_i^π	$E_{\text{level},f}$ (keV)	J_f^π	E_γ (keV)	I_γ	$I_\gamma^{\text{norm.}}$	$I_\gamma^{\text{norm.}}$ [10]
		0	0^+	**3636.6(3)**	0.43(3)	100(8)	
3673.46(18)	4^+	3057.15	2^+	**616.5(3)**	0.0133(18)	5.9(8)	
		2963.25	4^+	**710.2(4)**	0.009(4)	3.8(18)	
		2903.78	2^+	**769.7(3)**	0.035(3)	15.6(15)	
		2773.92	4^-	**899.7(3)**	0.032(6)	14(3)	
		2403.01	2^+	**1270.4(3)**	0.122(4)	54.8(18)	
		2327.82	2^+	**1345.6(3)**	0.082(8)	37(3)	
		2280.23	4^+	1393.3(3)	0.043(6)	19(3)	
		1229.50	2^+	2443.8(4)	0.22(3)	100(15)	
3690.4(3)	$3, 4, 5^-$	2773.92	4^-	**916.5(3)**	0.093(10)	53(6)	
		2403.01	2^+	**1287.2(3)**	0.0037(3)	2.12(16)	
		2324.77	3^-	**1365.6(3)**	0.176(8)	100(4)	
3695.98(14)	$1^+, 2^+$	2056.66	0^+	**1639.5(3)**	0.185(7)	28.3(11)	
		2042.67	2^+	**1653.3(3)**	0.115(10)	17.6(15)	
		1758.08	0^+	**1937.9(3)**	0.108(5)	16.5(8)	
		1229.50	2^+	2466.6(3)	0.339(18)	52(3)	
		0	0^+	3696.5(3)	0.65(16)	100(3)	
3699.31(17)	(2^+)	2737.89	1^+	**961.3(3)**	0.256(10)	49.4(18)	
		2496.78	0^+	**1202.1(4)**	0.0090(17)	1.7(3)	
		2403.01	2^+	**1296.0(3)**	0.004(2)	0.7(5)	
		2324.77	3^-	**1374.6(3)**	0.520(13)	100(3)	
		2280.23	4^+	**1418.4(3)**	0.033(3)	6.3(6)	
		0	0^+	**3699.7(3)**	0.12(3)	23(5)	
3709.99(19)	$(1^-, 2^+)$	2903.78	2^+	**806.3(3)**	0.016(2)	11.3(17)	
		2737.89	1^+	**972.1(3)**	0.142(5)	100(4)	
		2403.01	2^+	**1306.9(3)**	0.020(2)	14.0(15)	
		2324.77	3^-	**1385.3(3)**	0.126(5)	89(4)	
		2056.66	0^+	**1653.2(3)**	0.030(4)	21(3)	
		1758.08	0^+	**1951.9(3)**	0.016(3)	11.3(17)	
3728.2(4)	(2, 3)	2042.67	2^+	**1685.2(3)**	0.267(17)	100	
3737.66(19)	$(1,\ 2^+)$	3308.39	2^+	**429.5(3)**	0.016(3)	14(2)	
		2903.78	2^+	**834.2(3)**	0.057(3)	51(3)	
		2737.89	1^+	**1000.0(3)**	0.105(5)	93(4)	
		2496.78	0^+	**1240.9(3)**	0.088(5)	78(5)	
		2403.01	2^+	**1334.8(3)**	0.113(4)	100(4)	
		2042.67	2^+	**1695.2(3)**	0.061(5)	54(4)	
3761.98(13)	$(1^-, 2^+)$	2403.01	2^+	**1358.8(3)**	0.015(2)	1.07(18)	
		2327.82	2^+	**1434.1(3)**	0.069(8)	5.1(6)	
		2324.77	3^-	**1437.1(3)**	0.211(9)	15.6(7)	
		2042.67	2^+	**1719.2(3)**	0.31(2)	22.5(14)	
		1229.50	2^+	2532.3(3)	1.35(6)	100(5)	
		0	0^+	**3762.2(3)**		2.9(4)	
3770.8(2)	(3)	2737.89	1^+	**1032.8(4)**	0.012(2)	20(4)	
		2733.6	4^+	**1037.1(3)**	0.046(3)	69(4)	
		2403.01	2^+	**1367.7(3)**	0.0232(14)	78(5)	
		2280.23	4^+	**1490.6(3)**	0.067(6)	100(9)	
3816.17(3)	(4^+)	2488.57	4^+	1327.8(3)	0.030(4)	9.1(13)	21.8(26)
		2403.01	2^+	1413.6(3)	0.011(5)	3.2(14)	
		2280.23	4^+	1535.4(3)	0.0213(3)	6.5(8)	7.9(14)
		2042.67	2^+	**1774.1(3)**	0.055(14)	16.8(4)	
		1229.50	2^+	2586.9(3)	0.33(4)	100(11)	100(6)
3847.12(13)	(2^+)	2903.78	2^+	**943.3(3)**	0.019(5)	10(2)	
		2737.89	1^+	**1109.2(3)**	0.016(4)	9(2)	
		2677.20	2^+	**1169.9(3)**	0.022(6)	11.5(3)	
		2496.78	0^+	**1350.0(3)**	0.0108(15)	5.7(8)	
		2403.01	2^+	**1443.9(3)**	0.0461(3)	24.2(16)	

TABLE I. (*Continued.*)

$E_{\text{level},i}$ (keV)	J_i^π	$E_{\text{level},f}$ (keV)	J_f^π	E_γ (keV)	I_γ	$I_\gamma^{\text{norm.}}$	$I_\gamma^{\text{norm.}}$ [10]
		2324.77	3^-	**1522.3(3)**	0.190(6)	100(3)	
		2056.66	0^+	**1790.2(3)**	0.028(3)	14.8(17)	
		2042.67	2^+	**1804.0(4)**	0.039(5)	20(3)	
		1758.08	0^+	**2088.6(7)**	0.0064(19)	3.4(10)	
		1229.50	2^+	**2617.2(3)**	0.15(2)	76(13)	
		0	0^+	**3847.6(3)**	0.066(9)	35(5)	
3856.75(15)	2^+	3057.15	2^+	**799.9(7)**	0.0040(16)	0.9(4)	
		2677.20	2^+	**1179.4(4)**	0.038(10)	9(2)	
		2496.78	0^+	**1359.5(3)**	0.070(5)	16.3(11)	
		2280.23	4^+	**1577.3(3)**	0.018(3)	4.1(7)	
		2056.66	0^+	**1799.5(4)**	0.016(3)	3.8(8)	
		1758.08	0^+	2098.2(3)	0.024(2)	5.6(6)	
		1229.50	2^+	2627.1(3)	0.134(8)	30.8(19)	
		0	0^+	3857.0(3)	0.43(3)	100(6)	
3881.91(3)	(2)	3270.47	1	**611.2(3)**	0.0062(11)	0.88(15)	
		2324.77	3^-	**1556.9(3)**	0.710(18)	100	
3959.07(18)	$1^-,\ 2^+$	2737.89	1^+	**1221.2(3)**	0.210(10)	100(5)	
		2677.20	2^+	**1281.9(5)**	0.012(3)	5.5(16)	
		2324.77	3^-	**1634.0(3)**	0.037(3)	17.5(13)	
		2042.67	2^+	**1916.2(3)**	0.021(4)	10.1(18)	
		1229.50	2^+	**2729.8(3)**	0.180(6)	86(3)	
		0	0^+	**3959.0(3)**	0.070(9)	33(4)	
3972.3(3)	$1^-,\ 2^+$	2496.78	0^+	**1475.1(3)**	0.0278(17)	17.9(11)	
		2056.66	0^+	**1915.5(3)**	0.114(5)	73(3)	
		2042.67	2^+	**1929.5(3)**	0.156(11)	100(7)	
		1758.08	0^+	**2213.9(3)**	0.106(5)	68(4)	
3994.48(19)	$1^-,\ 2^+$	2677.20	2^+	**1317.3(3)**	0.022(3)	11.6(17)	
		2496.78	0^+	**1497.3(3)**	0.0125(16)	6.7(8)	
		2327.82	2^+	**1666.6(3)**	0.092(10)	49(5)	
		2324.77	3^-	**1669.9(3)**	0.026(4)	14(2)	
		2042.67	2^+	**1951.7(3)**	0.19(3)	100(15)	
4014.7(3)	(2)	3270.47	1	**744.0(4)**	0.0028(12)	1.3(6)	
		2324.77	3^-	**1689.7(3)**	0.218(11)	100	
4023.94(15)	(2^+)	2903.78	2^+	**1120.3(3)**	0.016(2)	17(2)	
		2677.20	2^+	**1346.7(3)**	0.018(3)	19(3)	
		2496.78	0^+	**1526.9(3)**	0.0219(13)	23.1(14)	
		2488.57	4^+	**1535.1(3)**	0.035(6)	37(7)	
		2403.01	2^+	**1621.0(3)**	0.013(2)	14(2)	
		2327.82	2^+	**1696.2(3)**	0.052(6)	55(6)	
		2324.77	3^-	**1699.1(3)**	0.060(6)	63(6)	
		2056.66	0^+	**1967.3(3)**	0.030(3)	31(4)	
		2042.67	2^+	**1981.7(3)**	0.028(4)	30(5)	
		1758.08	0^+	**2265.7(3)**	0.095(4)	100(4)	
4028.37(19)	(3^+)	3270.47	1	**758.0(3)**	0.0058(14)	2.3(5)	
		2903.78	2^+	**1124.5(3)**	0.013(2)	5.3(9)	
		2737.89	1^+	**1290.4(3)**	0.251(10)	100(4)	
		2677.20	2^+	**1351.0(3)**	0.051(4)	19.5(17)	
		2403.01	2^+	**1625.9(4)**	0.0039(13)	1.6(5)	
4034.41(19)	(3)	3057.15	2^+	**977.3(4)**	0.0102(17)	5.5(9)	
		2903.78	2^+	**1130.6(3)**	0.0201(3)	10.9(14)	
		2677.20	2^+	**1357.0(3)**	0.0206(3)	11.2(16)	
		2403.01	2^+	**1631.2(3)**	0.0098(18)	5.3(10)	
		2327.82	2^+	**1706.4(3)**	0.183(15)	100(8)	
4044.62(8)	$(1^+,\ 2^+,\ 3^+)$	2327.82	2^+	1716.5(3)	0.069(6)	22(2)	
		1229.50	2^+	2815.1(3)	0.313(14)	100(4)	
4108.88(17)	2^-	3057.15	2^+	**1051.3(3)**	0.044(6)	3.6(5)	

TABLE I. (*Continued.*)

$E_{\text{level},i}$ (keV)	J_i^π	$E_{\text{level},f}$ (keV)	J_f^π	E_γ (keV)	I_γ	$I_\gamma^{\text{norm.}}$	$I_\gamma^{\text{norm.}}$ [10]
		2773.92	4^-	**1334.7(3)**	0.065(5)	5.3(4)	
		2737.89	1^+	**1371.3(3)**	0.038(3)	3.1(3)	
		2677.20	2^+	**1431.3(5)**	0.07(3)	0.6(2)	
		2403.01	2^+	**1706.2(3)**	0.056(3)	4.6(3)	
		2042.67	2^+	**2066.9(3)**	0.123(9)	10.1(7)	
		1229.50	2^+	2879.0(3)	1.22(8)	100(4)	
4117.80(15)	(2^+)	2488.57	4^+	**1630.0(3)**	0.056(7)	4.6(6)	
		2403.01	2^+	**1714.3(3)**	0.074(5)	6.1(4)	
		2056.66	0^+	**2060.3(4)**	0.016(3)	1.3(2)	
		2042.67	2^+	**2075.8(3)**	0.209(18)	17.2(15)	
		1229.50	2^+	**2887.8(3)**	1.22(6)	100(13)	
		0	0^+	**4117.7(3)**	0.64(4)	53(3)	
4126.48(19)	$1^+,\ 2^+$	2496.78	0^+	**1628.4(4)**	0.0123(16)	1.7(2)	
		2403.01	2^+	**1722.7(5)**	0.016(2)	2.3(3)	
		2042.67	2^+	**2083.5(3)**	0.052(6)	7.3(9)	
		1758.08	0^+	**2368.0(3)**	0.048(3)	6.8(4)	
		1229.50	2^+	2897.3(3)	0.71(3)	100(5)	
		0	0^+	4126.4(3)	0.55(4)	77(5)	
4191.57(17)	$(2^-,\ 3^-)$	2773.92	4^-	**1417.7(3)**	0.028(6)	4.0(8)	
		2403.01	2^+	**1788.6(3)**	0.022(2)	3.1(4)	
		2327.82	2^+	**1863.1(3)**	0.259(19)	37(3)	
		2324.77	3^-	**1867.1(3)**	0.060(4)	8.6(5)	
		1229.50	2^+	**2961.8(3)**	0.70(6)	100(8)	
4226.6(2)	$(1,\ 2^+)$	1229.50	2^+	**2996.5(3)**	0.43(8)	100(19)	
		0	0^+	**4227.0(3)**	<0.17	<40	
4288.2(3)	(3)	1229.50	2^+	**3058.4(3)**	0.31(3)	100	
4299.7(4)	(2^+)	2042.67	2^+	**2256.8(3)**	0.163(13)	100(8)	
		1758.08	0^+	**2541.6(3)**	0.085(10)	53(6)	
4312.11(12)	$(1,\ 2^+)$	3761.98	$(1^-, 2^+)$	**550.1(3)**	0.067(4)	35(2)	
		3375.49	$(1,\ 2^+)$	**936.2(3)**	0.179(10)	94(5)	
		3308.39	2^+	**1003.6(3)**	0.020(4)	10(2)	
		3270.47	1	**1041.6(3)**	0.019(4)	9.8(19)	
		3228.27	2^+	**1083.7(3)**	0.0287(15)	15.1(8)	
		3057.15	2^+	**1255.0(3)**	0.078(3)	41.0(17)	
		2737.89	1^+	**1574.2(3)**	0.110(5)	58(3)	
		2677.20	2^+	**1634.9(3)**	0.089(7)	47(4)	
		2327.82	2^+	**1984.1(3)**	0.190(16)	100(9)	
		2042.67	2^+	**2270.0(3)**	0.088(9)	46(5)	
		1229.50	2^+	**3083.2(4)**	0.076(7)	40(4)	
4353.09(14)	$(1,\ 2^+)$	3270.47	1	**1082.8(4)**	0.007(3)	3.6(15)	
		2903.78	2^+	**1448.8(3)**	0.021(4)	1.9(4)	
		2496.78	0^+	**1856.6(4)**	0.0119(15)	1.08(14)	
		2403.01	2^+	**1950.5(6)**	0.023(9)	2.1(8)	
		2056.66	0^+	**2296.8(3)**	0.109(7)	9.9(6)	
		2042.67	2^+	**2310.7(3)**	0.39(3)	36(3)	
		1758.08	0^+	**2595.4(3)**	0.104(15)	9.5(14)	
		1229.50	2^+	**3122.8(3)**	1.10(5)	100(5)	
		0	0^+	**4353.5(3)**	0.167(13)	15.2(12)	
4406.21(19)	$(1,\ 2^+)$	2496.78	0^+	**1909.1(3)**	0.127(5)	22.2(9)	
		2403.01	2^+	**2003.1(3)**	0.035(4)	6.2(7)	
		2056.66	0^+	**2349.4(3)**	0.124(7)	21.7(12)	
		1758.08	0^+	**2647.8(3)**	0.018(3)	3.2(5)	
		1229.50	2^+	**3176.8(3)**	0.57(4)	100(8)	
4410.05(15)	$(1,\ 2^+)$	2042.67	2^+	**2367.2(3)**	0.31(2)	100(7)	
		1758.08	0^+	**2651.4(3)**	0.076(8)	24(2)	
4432.76(16)	$(1, 2^+)$	2496.78	0^+	**1935.4(3)**	0.044(3)	41(3)	

TABLE I. (*Continued.*)

$E_{\text{level},i}$ (keV)	J_i^π	$E_{\text{level},f}$ (keV)	J_f^π	E_γ (keV)	I_γ	$I_\gamma^{\text{norm.}}$	$I_\gamma^{\text{norm.}}$ [10]
		1758.08	0^+	**2674.8(3)**	0.060(5)	57(4)	
		1229.50	2^+	**3203.4(3)**	0.071(13)	67(12)	
		0	0^+	**4432.5(3)**	0.106(9)	100(9)	
4481.33(16)	$(1,\ 2^+)$	2737.89	1^+	**1743.4(5)**	0.018(4)	12(3)	
		2496.78	0^+	**1984.3(3)**	0.037(3)	25(2)	
		1758.08	0^+	**2722.8(3)**	0.073(4)	51(3)	
		1229.50	2^+	**3252.0(3)**	0.017(4)	11.5(3)	
		0	0^+	**4481.3(3)**	0.144(18)	100(12)	
4536.15(18)	$(1, 2^+)$	2042.67	2^+	**2493.4(3)**	0.093(8)	24(2)	
		1758.08	0^+	**2777.6(3)**	0.148(5)	38.8(14)	
		0	0^+	**4536.0(3)**	0.38(3)	100(8)	
4540.8(3)	$(3,\ 4^+)$	2327.82	2^+	**2212.9(3)**	0.119(10)	100(9)	
		2042.67	2^+	**2498.2(4)**	0.042(7)	31(6)	
4544.50(15)	$(1, 2^+)$	2496.78	0^+	**2047.4(4)**	0.0089(15)	1.6(3)	
		2403.01	2^+	**2141.4(3)**	0.094(5)	17.0(9)	
		2056.66	0^+	**2487.8(3)**	0.090(5)	16.3(8)	
		2042.67	2^+	**2501.6(3)**	0.206(14)	37.1(3)	
		1229.50	2^+	**3314.9(3)**	0.168(14)	30.2(3)	
		0	0^+	**4544.6(3)**	0.55(4)	100(7)	
4560.25(14)	$(1, 2^+)$	2737.89	1^+	**1823.1(5)**	0.0067(14)	2.6(6)	
		2677.20	2^+	**1883.5(3)**	0.014(4)	5.5(17)	
		2327.82	2^+	**2232.6(3)**	0.044(5)	17.00(19)	
		2056.66	0^+	**2503.5(3)**	0.133(10)	51(4)	
		1758.08	0^+	**2802.1(3)**	0.242(8)	93(3)	
		1229.50	2^+	**3329.7(3)**	0.261(11)	100(4)	
		0	0^+	**4560.4(3)**	0.207(13)	79(5)	
4585.00(14)	$(1, 2^+)$	2737.89	1^+	**1847.1(3)**	0.034(2)	26.8(19)	
		2677.20	2^+	**1907.7(3)**	0.013(5)	11(4)	
		2403.01	2^+	**2181.7(3)**	0.027(3)	22(2)	
		2056.66	0^+	**2528.5(3)**	0.125(5)	100(4)	
		2042.67	2^+	**2542.7(4)**	0.012(4)	10(3)	
		1758.08	0^+	**2827.1(3)**	0.108(4)	87(4)	
4667.8(4)	$3^{(-)}$	3270.47	1	**1397.4(3)**	0.191(6)	100.0(0)	
		2737.89	1^+	**1928.4(4)**	0.019(2)	10.2(12)	
4673.78(17)	$(1, 2^+)$	2403.01	2^+	**2270.1(4)**	0.016(3)	6.6(12)	
		2324.77	3^-	**2348.9(3)**	0.019(4)	7.9(16)	
		1229.50	2^+	**3444.4(3)**	0.247(9)	100(4)	
		0	0^+	**4673.4(3)**		<42	
4724.1(3)	$(1, 2^+, 3)$	1229.50	2^+	**3494.6(3)**	0.255(15)	100(6)	
4769.65(15)	$(2^-, 3^+)$	2903.78	2^+	**1865.9(3)**	0.042(11)	24(7)	
		2773.92	4^-	**1995.4(7)**	0.016(7)	9(4)	
		2737.89	1^+	**2031.8(3)**	0.159(7)	93(4)	
		2677.20	2^+	**2092.5(3)**	0.031(9)	18(5)	
		2403.01	2^+	**2366.5(3)**	0.172(5)	100(3)	
		2327.82	2^+	**2441.8(3)**	0.136(12)	79(7)	
4772.9(2)	$(2^+, 3)$	3270.47	1	**1502.4(3)**	0.111(4)	89(3)	
		2042.67	2^+	**2729.8(3)**	0.125(14)	100(11)	
		1229.50	2^+	**3543.2(4)**	0.077(16)	61(13)	
4834.14(7)	(1^+)	2327.82	2^+	**2507.0(3)**	0.146(11)	51(4)	
		2042.67	2^+	**2792.4(3)**	0.055(18)	19(6)	
		1229.50	2^+	**3605.2(3)**	0.111(10)	39(3)	
		0	0^+	**4834.0(4)**	0.286(18)	100(6)	
4848.02(19)	$(2^-, 3^+)$	4126.48	$1^+, 2^+$	**721.6(3)**	0.048(6)	32(4)	
		3695.98	$1,\ 2^+$	**1151.9(3)**	0.024(3)	15.8(17)	
		3270.47	1	**1577.6(3)**	0.041(2)	26.6(14)	
		2737.89	1^+	**2110.1(3)**	0.154(6)	100(4)	

TABLE I. (*Continued.*)

$E_{\text{level},i}$ (keV)	J_i^π	$E_{\text{level},f}$ (keV)	J_f^π	E_γ (keV)	I_γ	$I_\gamma^{\text{norm.}}$	$I_\gamma^{\text{norm.}}$ [10]
4899.5(3)	(3)	3270.47	1	**1629.1(3)**	0.065(2)	100(4)	
		2737.89	2^+	**2161.6(3)**	0.024(3)	38(4)	
4910.47(3)	(1, 2)	2677.20	2^+	**2233.4(4)**	0.015(4)	6.1(16)	
		2496.78	0^+	**2413.4(5)**	0.0065(15)	2.6(6)	
		2403.01	2^+	**2507.5(3)**	0.089(5)	35.5(18)	
		2327.82	2^+	**2582.6(3)**	0.251(18)	100(7)	
4919.4(3)	$(1, 2^+)$	2056.66	0^+	**2862.4(3)**	0.202(6)	100	
4981.40(16)	$(1, 2^+)$	2403.01	2^+	**2578.1(3)**	0.020(2)	14.1(17)	
		2327.82	2^+	**2653.3(3)**	0.036(5)	26(4)	
		2056.66	0^+	**2924.4(3)**	0.056(4)	40(3)	
		2042.67	2^+	**2938.4(3)**	0.060(8)	42(5)	
		1229.50	2^+	**3752.3(3)**	0.141(11)	100(8)	
4999.0(3)	$(1,\ 2^+)$	2056.66	0^+	**2941.9(3)**	0.046(2)	61(3)	
		2042.67	2^+	**2956.2(3)**	0.028(8)	37(10)	
		1758.08	0^+	**3240.5(3)**	0.037(2)	49(3)	
		1229.50	2^+	**3769.3(6)**	0.075(11)	100(14)	
5006.35(15)	$(1,\ 2^+)$	2056.66	0^+	**2949.5(5)**	0.011(3)	11(3)	
		2042.67	2^+	**2963.4(3)**	0.024(8)	22(8)	
		1758.08	0^+	**3247.7(3)**	0.056(2)	52(2)	
		1229.50	2^+	**3776.6(3)**	0.106(9)	100(9)	
5089.70(15)	$(1,\ 2^+)$	2496.78	0^+	**2592.8(3)**	0.014(3)	8.2(15)	
		2042.67	2^+	**3047.5(3)**	0.117(9)	68(5)	
		1758.08	0^+	**3331.6(3)**	0.039(3)	22.3(16)	
		1229.50	2^+	**3860.2(3)**	0.173(8)	100(5)	
		0	0^+	**5089.6(3)**	0.09(2)	52(11)	
5119.30(18)	$(1,\ 2^+)$	2903.78	2^+	**2215.7(5)**	0.009(2)	6.7(16)	
		2056.66	0^+	**3062.5(3)**	0.075(3)	55(2)	
		2042.67	2^+	**3076.5(3)**	0.130(9)	97(7)	
		1758.08	0^+	**3360.5(4)**	0.011(2)	8.2(17)	
		1229.50	2^+	**3890.2(3)**	0.135(13)	100(10)	
5123.9(4)	(3^+)	2737.89	1^+	**2385.9(3)**	0.093(4)	100	
5152.3(2)	(3^+)	3856.75	2^+	**1295.9(3)**	0.036(13)	43(16)	
		3270.47	1	**1882.1(7)**	0.0241(19)	29(2)	
		2737.89	1^+	**2414.5(3)**	0.084(13)	100(16)	
5180.9(5)	$(1,\ 2^+)$	3270.47	1	**1910.0(3)**	0.0031(11)	4.5(17)	
		3251.9	(3^+)	**1929.3(3)**	0.0065(19)	10(3)	
		3228.27	2^+	**1953.3(3)**	0.0055(19)	8(3)	
		2403.01	2^+	**2777.8(3)**	0.042(3)	62(4)	
		2056.66	0^+	**3124.1(3)**	0.068(3)	100(4)	
		2042.67	2^+	**3138.6(3)**	0.036(3)	53(5)	
5193.38(17)	$(1,\ 2^+)$	2403.01	2^+	**2790.3(3)**	0.028(3)	28(3)	
		1758.08	0^+	**3435.0(3)**	0.009(3)	9(3)	
		1229.50	2^+	**3964.7(3)**	0.080(14)	80(14)	
		0	0^+	**5193.0(3)**	0.10(4)	100(4)	
5232.82(19)	$(1, 2^+)$	2056.66	0^+	**3176.3(3)**	0.026(3)	36(4)	
		2042.67	2^+	**3190.3(3)**	0.070(11)	100(14)	
		1758.08	0^+	**3474.6(3)**	0.038(2)	53(3)	
5244.00(19)	$(1, 2^+)$	1758.08	0^+	**3486.4(3)**	0.021(5)	41(9)	
		0	0^+	**5244.0(3)**	0.052(3)	100(5)	
5274.28(17)	$(1, 2^+)$	2056.66	0^+	**3217.4(3)**	0.034(3)	10.3(8)	
		2042.67	2^+	**3232.2(3)**	0.073(7)	22(2)	
		1229.50	2^+	**4044.9(3)**	0.33(2)	100(6)	
		0	0^+	**5274.0(3)**	0.094(5)	28(14)	
5323.49(18)	$(1,\ 2^+)$	2327.82	2^+	**2995.9(3)**	0.064(5)	52(4)	
		1758.08	0^+	**3565.6(3)**	0.0408(3)	33(2)	

TABLE I. (*Continued.*)

$E_{\text{level},i}$ (keV)	J_i^π	$E_{\text{level},f}$ (keV)	J_f^π	E_γ (keV)	I_γ	$I_\gamma^{\text{norm.}}$	$I_\gamma^{\text{norm.}}$ [10]
		0	0^+	**5323.1(3)**	0.123(6)	100(5)	
5382.8(2)	$(1,\ 2^+)$	2496.78	0^+	**2886.6(3)**	0.034(2)	15.1(10)	
		0	0^+	**5382.6(3)**	0.227(14)	100(6)	
5396.24(19)	$(1, 2^+)$	2496.78	0^+	**2899.5(3)**	0.020(19)	14.4(14)	
		2056.66	0^+	**3339.7(3)**	0.038(3)	27.5(19)	
		0	0^+	**5396.3(3)**	0.139(8)	100(6)	
5524.9(2)	$(1,\ 2^+)$	1229.50	2^+	**4295.2(3)**	0.040(9)	22(5)	
		0	0^+	**5524.8(3)**	0.178(8)	100(5)	
5549.3(2)	$(1,\ 2^+)$	1229.50	2^+	**4320.1(3)**	0.107(7)	100(6)	
		0	0^+	**5549.9(4)**	< 0.05	< 81	
5613.75(19)	$(1, 2^+)$	2403.01	2^+	3210.5(4)	0.007(2)	4.8(15)	
		1229.50	2^+	**4384.6(3)**	0.143(7)	100(5)	
		0	0^+	**5613.4(3)**	0.043(5)	30(4)	
5851.40(16)	$(1,\ 2^+)$	3695.98	$1, 2^+$	**2156.6(3)**	0.0126(12)	7.7(8)	
		2403.01	2^+	**3450.0(4)**	0.019(4)	12(2)	
		2042.67	2^+	**3808.3(3)**	0.123(10)	71(6)	
		1758.08	0^+	**4093.8(3)**	0.023(2)	14.1(12)	
		1229.50	2^+	**4621.9(3)**	0.165(6)	100(4)	
		0	0^+	**5852.2(4)**	0.087(7)	53(4)	
6004.1(2)	$(1,\ 2^+)$	1229.50	2^+	**4774.4(3)**	0.097(7)	100(7)	
		0	0^+	**6004.0(3)**	0.076(8)	78(8)	
6168.40(18)	$(1,\ 2^+)$	2403.01	2^+	**3766.7(4)**	0.016(3)	12(2)	
		2042.67	2^+	**4124.9(3)**	0.045(7)	33(5)	
		0	0^+	**6167.9(3)**	0.135(7)	100(5)	
6305.59(13)	$(1^-,\ 2^+)$	2737.89	1^+	**3567.7(3)**	0.0123(17)	8.6(12)	
		2403.01	2^+	**3902.4(5)**	0.016(3)	11(2)	
		2327.82	2^+	**3977.6(3)**	0.076(6)	54(5)	
		2324.77	3^-	**3981.5(4)**	0.048(4)	34(3)	
		2042.67	2^+	**4262.2(3)**	0.143(10)	100(7)	
		1758.08	0^+	**4548.1(3)**	0.082(3)	57(2)	
		1229.50	2^+	**5075.2(3)**	0.034(2)	23.8(14)	
		0	0^+	**6305.5(3)**	0.025(3)	17(2)	
9326.23(7)	$(0^+,\ 1^+)$	6305.59	$(1^-,\ 2^+)$	**3021.6(3)**	0.41(7)	11.5(19)	
		6168.40	$(1,\ 2^+)$	**3158.2(3)**	0.212(9)	6.0(3)	
		6004.1	$(1,\ 2^+)$	**3322.0(3)**	0.148(1)	4.1(3)	
		5613.75	$(1,\ 2^+)$	**3712.5(3)**	0.199(11)	5.6(3)	
		5549.3	$(1,\ 2^+)$	**3776.7(3)**	0.106(9)	2.98(3)	
		5524.9	$(1,\ 2^+)$	**3801.2(3)**	0.305(13)	8.5(4)	
		5396.24	$(1,\ 2^+)$	**3930.3(3)**	0.134(12)	3.8(3)	
		5382.8	$(1,\ 2^+)$	**3943.7(3)**	0.16(2)	4.5(6)	
		5323.49	$(1,\ 2^+)$	**4002.8(3)**	0.28(3)	7.7(7)	
		5274.28	$(1,\ 2^+)$	**4052.2(3)**	0.54(5)	15.1(14)	
		5244.00	$(1,\ 2^+)$	**4082.4(3)**	0.060(7)	1.7(2)	
		5232.82	$(1,\ 2^+)$	**4093.6(3)**	0.073(10)	2.1(3)	
		5193.38	$(1,\ 2^+)$	**4133.0(3)**	0.184(15)	5.1(4)	
		5180.9	(3^+)	**4146.1(3)**	0.047(3)	1.32(9)	
		5152.3	(3^+)	**4174.2(3)**	0.18(3)	4.9(8)	
		5123.9	(3^+)	**4202.5(3)**	0.0158(10)	0.44(3)	
		5119.30	$(1,\ 2^+)$	**4206.8(3)**	0.139(12)	3.9(3)	
		5089.70	$(1,\ 2^+)$	**4236.9(3)**	0.36(9)	10(3)	
		4981.40	$(1,\ 2^+)$	**4344.3(3)**	0.15(2)	4.2(6)	
		4919.4	$(1,\ 2^+)$	**4406.9(3)**	0.094(5)	2.63(14)	
		4899.5	$(1,\ 2^+)$	**4426.5(3)**	0.074(5)	2.01(15)	
		4848.02	$(1,\ 2^+)$	**4478.1(3)**	0.26(2)	7.4(6)	
		4834.14	$(1,\ 2^+)$	**4491.2(3)**	0.58(10)	16(3)	
		4772.9	$(2^+,\ 3^+)$	**4553.1(3)**	0.082(5)	2.28(14)	

TABLE I. (*Continued.*)

$E_{\text{level},i}$ (keV)	J_i^π	$E_{\text{level},f}$ (keV)	J_f^π	E_γ (keV)	I_γ	$I_\gamma^{\text{norm.}}$	$I_\gamma^{\text{norm.}}$ [10]
		4769.65	$(2^-,\ 3^+)$	**4556.4(3)**	0.39(2)	11.0(5)	
		4724.1	$(1,\ 2^+)$	**4601.7(3)**	0.144(6)	4.07(18)	
		4673.78	$(1,\ 2^+)$	**4652.0(3)**	0.210(16)	5.9(4)	
		4667.8	$(1,\ 2^+)$	**4658.1(3)**	0.153(5)	4.28(15)	
		4585.00	$(1,\ 2^+)$	**4741.4(3)**	0.15(2)	4.3(6)	
		4560.25	$(1,\ 2^+)$	**4765.6(3)**	0.74(5)	20.8(13)	
		4544.50	$(1,\ 2^+)$	**4781.6(3)**	0.54(10)	15(3)	
		4536.15	$(1,\ 2^+)$	**4789.4(3)**	0.59(11)	17(3)	
		4841.33	$(1,\ 2^+)$	**4844.3(3)**	0.119(6)	3.33(16)	
		4432.76	$(1,\ 2^+)$	**4893.0(3)**	0.108(8)	3.0(2)	
		4410.05	$(1,\ 2^+)$	**4917.1(3)**	0.135(5)	3.77(15)	
		4406.21	$(1,\ 2^+)$	**4919.7(3)**	0.459(19)	12.8(5)	
		4953.09	$(1,\ 2^+)$	**4973.4(3)**	0.98(15)	27(4)	
		4312.11	$(1,\ 2^+)$	**5013.7(3)**	0.80(14)	22(4)	
		4299.7	(2^+)	**5028.3(3)**	0.073(4)	2.03(11)	
		4288.2	(3)	**5037.4(4)**	0.119(4)	3.33(12)	
		4226.6	$(1,\ 2^+)$	**5099.5(3)**	0.41(10)	11(3)	
		4191.57	$(2^-,\ 3^-)$	**5134.2(3)**	0.52(8)	15(2)	
		4126.48	$1^+,\ 2^+$	**5200.0(3)**	0.137(7)	3.85(18)	
		4117.80	2^+	**5208.4(3)**	1.03(4)	28.9(11)	
		4108.88	2^-	**5217.2(3)**	0.93(6)	25.9(17)	
		4044.62	$(1^+,\ 2^+,\ 3^+)$	**5281.2(3)**	0.073(3)	2.04(8)	
		4034.41	(3)	**5291.4(3)**	0.043(3)	1.21(8)	
		4028.37	(3^+)	**5297.4(3)**	0.194(12)	5.4(3)	
		4023.94	2^+	**5302.0(3)**	0.0166(15)	0.47(4)	
		4014.7	(2)	**5311.1(3)**	0.098(7)	2.75(18)	
		3994.48	$(1^-,\ 2^+)$	**5331.3(3)**	0.064(3)	1.78(10)	
		3959.07	$(1^-,\ 2^+)$	**5366.7(3)**	0.084(4)	2.34(11)	
		3881.91	(2)	**5444.0(3)**	0.46(3)	13.00(9)	
		3856.75	2^+	**5469.0(3)**	0.145(16)	4.1(5)	
		3847.12	(2^+)	**5478.5(3)**	0.126(10)	3.5(3)	
		3761.98	$(1^-,\ 2^+)$	**5563.8(3)**	0.77(10)	22(3)	
		3737.66	$(1,\ 2^+)$	**5587.7(3)**	0.032(12)	0.9(3)	
		3699.31	(2^+)	**5626.4(3)**	0.50(3)	13.9(9)	
		3636.49	$(1^-,\ 2^+)$	**5689.5(3)**	0.24(16)	6.6(5)	
		3623.5	(2^+)	**5703.7(3)**	0.034(2)	0.96(6)	
		3586.5	(2^+)	**5738.7(3)**	0.37(3)	10.5(8)	
		3528.7	(2^+)	**5797.5(3)**	0.038(3)	1.07(9)	
		3462.92	(2^+)	**5863.3(3)**	0.34(3)	9.5(8)	
		3375.49	(1)	**5950.2(3)**	0.147(11)	4.1(3)	
		3355.59	2^+	**5970.9(3)**	0.34(4)	9.5(11)	
		3352.9	$0^{(+)}$	**5972.6(3)**	0.29(3)	8.1(8)	
		3308.39	2^+	**6017.5(3)**	0.110(5)	3.07(14)	
		3270.47	1	**6055.4(3)**	0.61(3)	17.1(8)	
		3262.33	3^+	**6063.4(3)**	0.0403(18)	1.13(5)	
		3228.27	2^+	**6096.9(3)**	0.23(2)	6.4(6)	
		3215.87	(0^+)	**6109.8(5)**	0.74(5)	20.7(14)	
		3137.35	0^+	**6188.6(3)**	0.056(6)	1.58(15)	
		3057.15	2^+	**6268.7(3)**	0.056(3)	1.56(9)	
		2903.78	2^+	**6422.1(3)**	1.13(9)	31.5(3)	
		2737.89	1^+	**6588.0(3)**	0.147(15)	4.1(4)	

TABLE I. (*Continued.*)

$E_{\text{level},i}$ (keV)	J_i^π	$E_{\text{level},f}$ (keV)	J_f^π	E_γ (keV)	I_γ	$I_\gamma^{\text{norm.}}$	$I_\gamma^{\text{norm.}}$ [10]
		2677.20	2^+	**6648.7(3)**	0.93(7)	26.0(18)	
		2496.78	0^+	**6828.8(3)**	0.41(3)	11.4(9)	
		2403.01	2^+	**6922.9(3)**	0.113(9)	3.2(3)	
		2327.82	2^+	**6998.1(3)**	0.32(2)	9.0(6)	
		2056.66	0^+	**7269.2(3)**	0.46(4)	12.8(11)	
		2042.67	2^+	**7283.0(3)**	0.215(2)	6.0(6)	
		1758.08	0^+	**7568.0(3)**	0.028(3)	0.78(9)	
		1229.50	2^+	**8096.7(3)**	0.33(3)	9.1(8)	
		0	0^+	**9326.2(3)**	3.6(4)	100(11)	

with the intensity and the γ-decay pattern in the present experiment.

The capture state is treated as a continuum of 0^+ and 1^+ states from which the primary γ-ray transitions populate energy levels with spins, generally, less than $J = 3$. The most intense primary transition is a 9326-keV transition directly to the ground state with a relative intensity of 3.6(4)% of the 1229.7-keV transition from the first excited 2^+ state. The 9326-keV transition is evident from the singles spectrum shown in Fig. 1. In the ^{115}Sn$(n,\gamma)^{116}$Sn experiment of Ref. [27], the capture state populated the ground state directly with a relative intensity of of 0.18(4)%, which may suggest that most captures occurred in a 0^+ state.

Based on the experimental observations in the PQR studies of ^{124}Sn [19], and ^{112,114}Sn [20], a potential signature of these PQR states is an enhanced ground-state branching fraction, b_0. In these studies, $b_0 \geqslant 0.5$ is observed for states suggested to belong to the PQR. The large ground-state branching ratios are not reflective of pure quadrupole-multiphonon excitations but rather are indicative of major one-phonon excitations to excited 2^+ states. The present experiment identified 33 levels which directly populate the ground state and could have $J^\pi = 2^+$. Fig. 2 shows the ground-state branching fraction of these selected states. Internal conversion coefficients were not factored in determining the intensity balance. This was because the γ-ray transitions, all being greater than 500 keV, dominate the transition strength compared to internal conversion.

All newly observed transitions were placed using γ-γ coincidences. An example of the projected spectrum from gating on the 1230-keV transition from the first excited 2^+ is shown in Fig. 3. The γ-γ coincidences were also used to investigate the isotopic contamination present in the target. The most significant γ-ray contaminants were from the ^{115,119}Sn(n,γ) reactions. This was primarily due to the large thermal neutron-capture cross section of 30(7) b of ^{115}Sn [23], and the relatively large abundance and thermal neutron-capture cross section of 8.59% [28] and 2.2(5) b [23] of ^{119}Sn, respectively. However, each of these contaminants resulted in less than 1% of the total γ-ray spectrum and were not investigated further.

The spin assignments for newly identified states were based primarily on γ-decay selection rules. It was not possible to rule out spins $J = 1$, but, for those that γ decay directly to the ground state, the spin cannot be $J = 0$ and is unlikely to be $J = 3$. Angular correlations were considered for the states

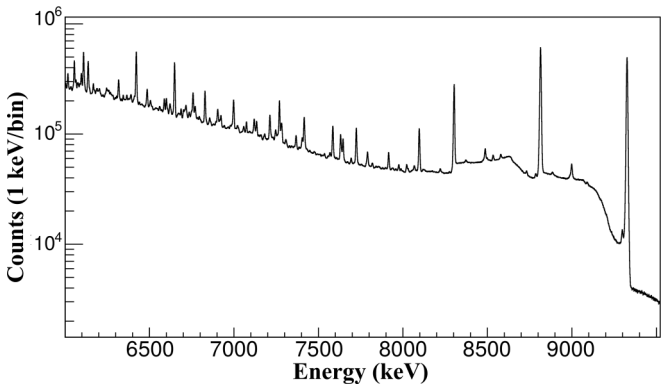

FIG. 1. The high energy region of the singles γ spectrum using addback that was populated in the present ^{117}Sn$(n,\gamma)^{118}$Sn experiment. The spectrum was put in logarithmic scale to accentuate the photopeaks. The highest energy photopeak corresponds with the 9326-keV transition to the ground state from the capture state.

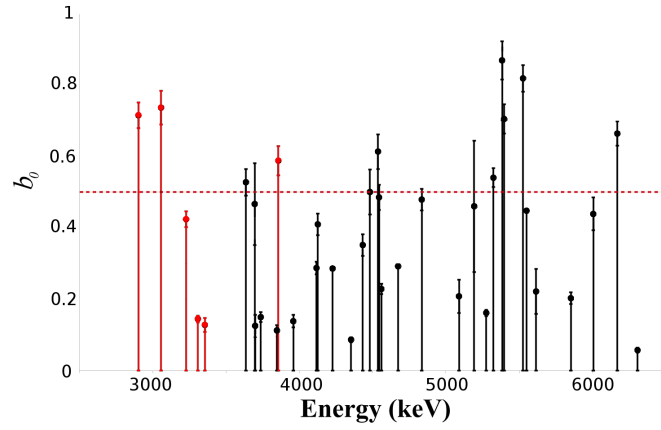

FIG. 2. The absolute branching fraction of the ground state transition from states in the proposed PQR region. The levels in red are known to be $J = 2^+$, whereas the spins of the other levels are not presently known. The red dashed line represents $b_0 = 0.5$. It is suggested that PQR states are ground state excitations which would predominantly decay to the ground state [19,20].

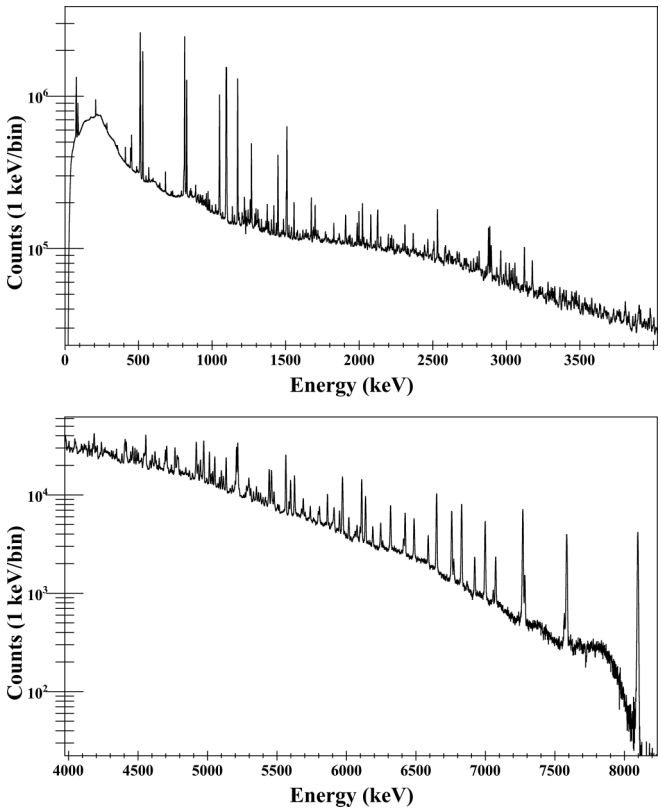

FIG. 3. The 1230-keV gated projection used to identify transitions in coincidence with the 1230-keV ground-state transition. Shown is the energy region of 0–4000 keV set to logarithmic scale for clarity.

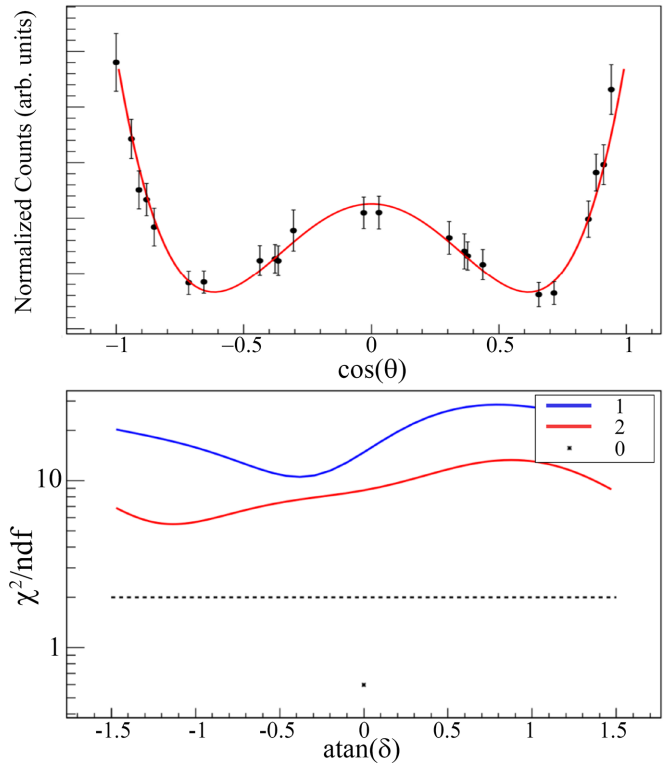

FIG. 4. The γ-γ angular correlation (top) for the 1700-keV $\rightarrow$ 1230-keV cascade is shown from which a spin of $J = 0$ was assigned to the 2929-keV level. The χ^2 minimization (bottom) rules out a possible $J = 1^+$ which was previously given [24]. The dotted line represents the 3σ limit.

in the PQR region; however, due to low statistics of these transitions, this kind of analysis was not possible.

The most intense transitions for which angular correlations measurements could be performed generally originate from states with already known spins. However, four states have been given firm spin assignment based on angular correlations: a previously known level at 2929.6 keV and three newly observed levels at 3216, 3353, and 3375 keV. The 3375-keV level was determined to have a spin of $J = 1$ while the other three were all assigned as $J = 0$ based on the angular correlations of the present experiment, as shown in Figs. 4–7.

The angular correlations were evaluated using the formula, $W(\theta) = A_{00}[1 + a_2P_2(\cos\theta) + a_4P_4(\cos\theta)]$. The theoretical coefficients, a_2 and a_4, were calculated for all possible mixing ratios using the ANGULAR CORRELATION UTILITY [29] in order to obtain χ^2-minimization plots for each of the potential spins. Only the FIPPS detectors were considered in the angular correlations, which provide 23 unique angles between detector pairs. The reason for this is that the IFIN detectors were at a distance of 20 cm, compared to 9 cm for FIPPS. The angular correlations were normalized using the event-mixed technique which is outlined in great detail in Ref. [30].

It was also necessary to determine the attenuation of the angular correlations, which was done by fitting three different and known $0 \rightarrow 2 \rightarrow 0$ angular correlations in which both γ-ray transitions are pure $E2$. The attenuation factors, or q values, were determined by comparing the fitted values for a_2 and a_4 and comparing them to the theoretical values, $a_2 = 0.36$ and $a_4 = 1.14$. All three cascades used involved the 1230-keV transition from the first 2^+ state to the 0^+ ground state. The other pure $E2$ transitions were 528, 827, and 1267 keV from the 0^+ levels at 1758, 2057, and 2497 keV, respectively. The weighted average of these values was determined to be, $q_2 = 0.95(2)$ and $q_4 = 0.843(7)$.

Angular correlations of four transitions with known mixing ratios were measured as a means to further test the q values. The results are summarized in Table II and show good agreement with literature.

For the spin assignment of $J = 1$ to the 3375-keV level, the 1098-keV transition from the 2328-keV, $J = 2^+$ level was used with the previously measured mixing ratio of $\delta = -14(4)$ [10]. The resulting χ^2 minimization plot in Fig. 7 produced a mixing ratio for the 1048-keV transition of $\delta = 0.67(10)$.

IV. $E0$ TRANSITIONS

Enhanced $\rho^2(E0)$ strengths are a potential signature of shape coexistence [31]. However, it is often a difficult task to measure the $E0$ transition intensity because of the need for measuring conversion electrons. In the present experiment, an indirect measurement of a known 299-keV, $E0$ transition connecting the 0_3^+ to the 0_2^+ was performed using the γ-ray

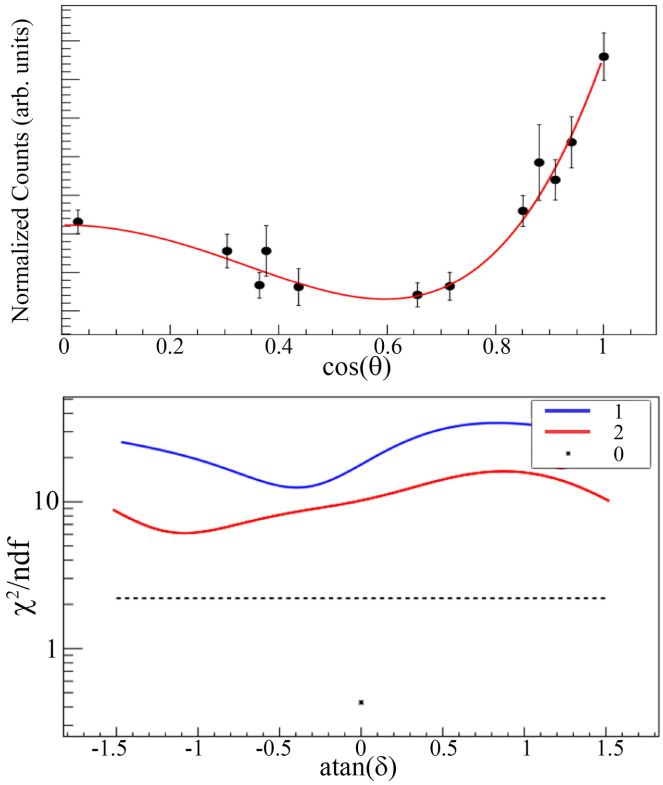

FIG. 5. The γ-γ angular correlation (top) for the 1987-keV $\rightarrow$ 1230-keV cascade is shown. Based on the χ^2 minimization plot (bottom), a spin of $J_i = 0$ was assigned to the 3216-keV level. The angles between detector pairs were folded about the y axis to enhance the statistics.

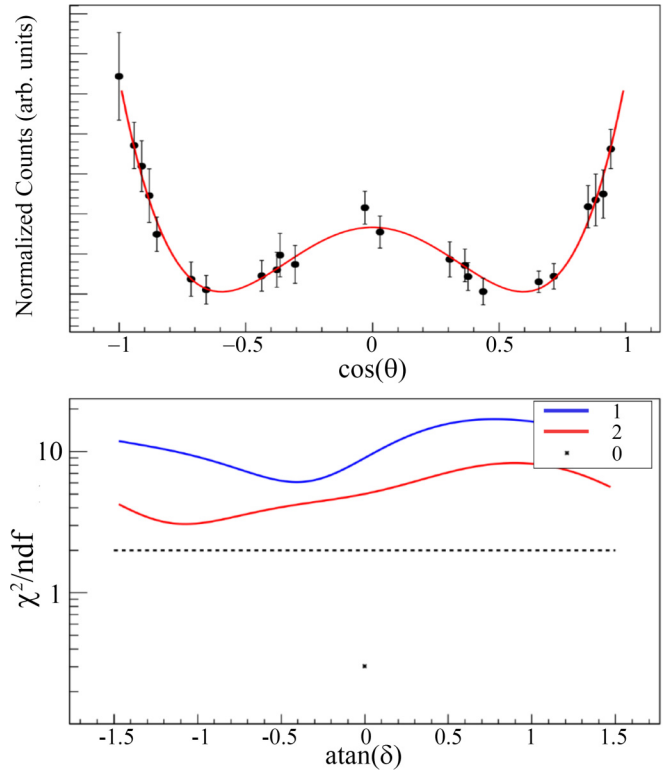

FIG. 6. The γ-γ angular correlation (top) for the 2123-keV $\rightarrow$ 1230-keV cascade. A spin assignment of $J_i = 0$ for the 3353-keV level was given based on the χ^2 minimization plot (bottom).

intensity of the known 528-keV, $E2$ transition from the 0_2^+ to the 2_1^+.

Gating on the 7269-keV transition (shown in Fig. 8), which populates the 0_3^+, 2057-keV level, revealed the 528-keV transition that decays from the 2p-2h, 1758-keV, 0_2^+ level to the 1230-keV, 2_1^+ level. This indicates an unobserved 299-keV, $E0$, $0_3^+ \rightarrow 0_2^+$ transition. Assuming that all intensity of the 299-keV transition is captured in the 528-keV photopeak, it is possible to obtain the branching ratio between the unobserved 299-keV transition and the 827-keV, $E2$ transition to the 2_1^+ level. The branching ratio of the 299-keV transition was determined to be 2.5(2)% of the 827-keV transition.

Following the equations outlined in Ref. [32], the quantities $q_K^2(E0/E2)$, $X(E0/E2)$, and $\rho^2(E0)$ were determined from the indirectly measured intensity of the 299-keV, $E0$ transition and with the relevant electronic factors calculated with BRICC [33]. The measured $q_K^2(E0/E2)$ and $X(E0/E2)$ were determined to be 12.7(11) and 6.3(5), respectively, compared to 8.4(19) and 4.2(10), respectively in Ref. [32]. This shows a slightly greater $E0$ strength in the present measurement. The $10^3 \times \rho^2(E0)$ value was calculated to be >38. The 2057-keV level has a mean half-life of <200 ps which limits the $\rho^2(E0)$ value to a lower limit. In Ref. [32], $10^3 \times \rho^2(E0) > 36$. However, it is likely that this should be >26 which can be determined from their referenced value of $q_K^2(E0/E2) = 8.4(19)$ as well as the realization that the <200 ps half-life would produce >36 and the lifetime of <288.5 ps, which is used in these calculations, produces >26.

Until the lifetime of the 2057-keV level is more precisely known, it is unclear how much strength the $0_3^+ \rightarrow 0_2^+$, $E0$ transition has. However, there is good reason to tabulate the intensity ratios of the $E0$ to the $E2$ in the form of $q_K^2(E0/E2)$ for low-lying 0^+ states which can then be used later to calculate the $\rho^2(E0)$ values when lifetime measurements are known. Based on the present measurements, γ-ray spectroscopy shows to be useful in obtaining $E0$ strength.

V. THEORETICAL CALCULATIONS

The microscopic and accurate calculation of the nuclear level density has been a great challenge due to the complexity of nucleon interaction and the exponential increase in the number of levels and configurations with increasing excitation energy. The shell model configuration interaction approach with exact diagonalization would be the most suitable method to confront that challenge but is rarely performed except for light nuclei due to the computation limitation. Phenomenological and extrapolated methods are used instead. In this paper, large-scale shell model (LSSM) calculations were performed for ^{118}Sn in the model space which includes all orbitals between $N = 50$ and 82 ($g_{7/2}$, $d_{5/2,3/2}$, $s_{1/2}$, and $h_{11/2}$) to derive all the possible low-lying states within the space. A monopole optimized realistic nucleon-nucleon interaction from Ref. [34] was employed. The bases were firstly

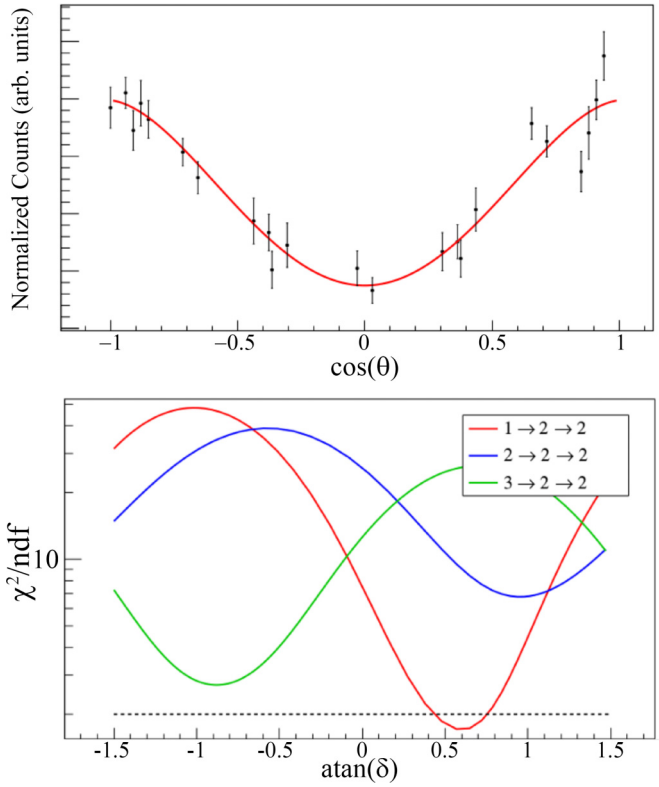

FIG. 7. The γ-γ angular correlation (top) for the 1048-keV $\rightarrow$ 1098-keV cascade. A spin assignment of $J_i = 1$ was given to the 3375-keV level and a mixing ratio of $\delta = 0.67(10)$ for the 1048-keV transition was measured based on the χ^2 minimization plot (bottom).

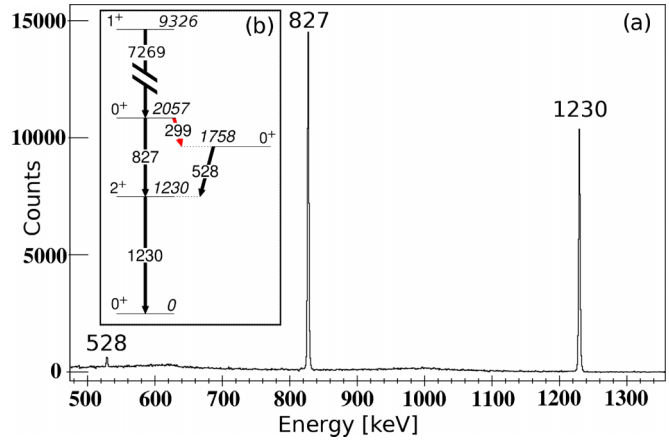

FIG. 8. From γ-γ coincidences, an unobserved 299-keV, $E0$ transition (red arrow) was indirectly measured by gating on the 7269-keV primary transition which feeds the 0_3^+, 2057-keV level from the capture state (b). This yields a spectra (a) with a dominant 827-keV transition that feeds the 2_1^+, 1230-keV level and a much weaker 528-keV photopeak that indicates the $E0$ transition connecting the 0_3^+ to the 2p-2h 0_2^+.

constructed in the so-called M-scheme without explicit angular momentum conservation. In principle one should be able to get all the low-lying states with different spin values after diagonalization with the Lanczos iteration approach starting with a random Lanczos vector. The calculation will, however, become more and more difficult as the number of iterations increases. Therefore, an angular momentum projection on the trial Lanczos vector was first performed. As a result, all of the Lanczos vectors generated in the interaction, and consequently the eigenstates, conserved angular momentum. With that, the lowest-lying states for each angular momentum and parity were calculated separately. There were 200 Lanczos vectors included for each calculation and the calculation was stopped after the lowest 10–50 states fully converged.

In addition, we have performed generalized seniority calculations with the same Hamiltonian considering a truncated shell model space including states with maximum seniority $\nu = 8$ as in Ref. [3]. The truncation allowed all possible states within the model space to be calculated. In practice, all states up to 6 MeV excitation energy are projected.

TABLE II. Four experimentally determined mixing ratios, δ for transitions between $J = 2$ and the 1230-keV level were performed to test the q values. The measured mixing ratios are in good agreement with the previous measured values from the recent β-decay experiment [10] as well as with the evaluated data.

Transition (keV)	δ_{exp}	χ^2_ν	δ_β [10]	δ_{lit} [24]
813	−2.27(12)	0.66	−2.28(7)	−2.34(16)
1098	−8.2(12)	0.34	−14(4)	56(31)
1173	0.83(5)	0.14	0.85(3)	1.07(9)
1447	2.8(4)	1.0		2.46^{17}_{13}

VI. DISCUSSION

It is suggested that the capture state is predominantly $J = 1^+$ based on the strong ground-state decay via the 9326-keV γ-ray emission which has a relative intensity of 3.6(4). This spin assignment was also previously suggested in Ref. [26], in which the ground-state branching was measured to be 5.3(8). From a 1^+ capture state, it was expected that primary transitions will populate states with $J = 0, 1, 2$ with both positive and negative parities, and 3^+ states from an $E2$ primary transition. For the low-lying excited states with known spin and parity, this is what was observed.

For both the shell-model and seniority-scheme calculations, the level density of all states up to 6 MeV with $J = 0$, 1, and 2 as well as the lowest three energy levels for $J = 3, 4$, and 5 is considerably less than what is experimentally observed in the 3–4 MeV region as shown in Fig. 9. Including all levels with $J = 3$, 4, and 5 for both calculations will reproduce the density in the 3–4 MeV region. However, the density in the 4–6 MeV region is then much more enhanced. It is reasonable to assume the experimentally observed levels will have spins less than $J = 3$.

Comparisons to the theoretical calculations for the low-spin states, $J = 0$, 1, and 2, provide some support for the experimentally observed states in the 3–5 MeV region to be $J = 2^+$ as both the *gdsh*-LSSM and generalized seniority

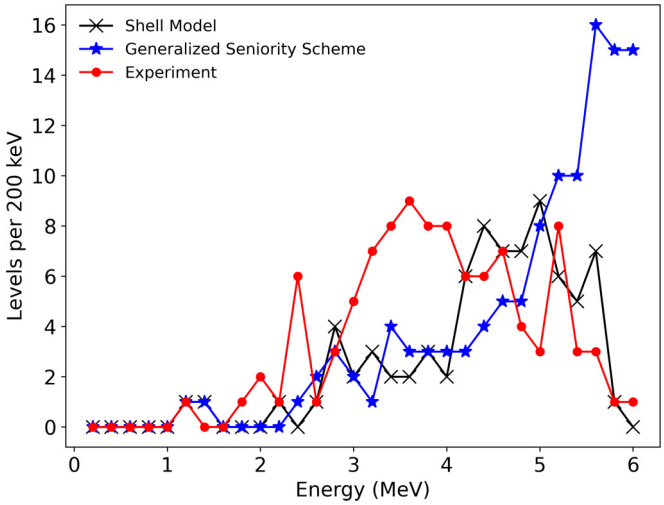

FIG. 9. Number of levels per 200 keV for the experimentally observed levels, and the shell-model and seniority-scheme calculated levels up to 6 MeV. The calculated levels consist of all calculated $J = 0$, 1, and 2 levels and only the lowest three levels for $J = 3$, 4, and 5 as it is unlikely that many observed states have spins greater than $J = 2$.

calculations predict a greater density of 2^+ states than the $J = 1^+$, 1^-, or 2^- states in the PQR region. This is shown in Fig. 10. For instance, in the 3–5 MeV range, the numbers of 2^+ states predicted by the shell-model and the general-seniority calculations are 34 and 26, respectively. Considering only the 1^+ and 1^- states (2^- is not as favorable based on the ground state transitions), the totals are then 25 and 14, respectively.

Generally, both sets of calculations predict higher energies for negative-parity states, which is due to the promotion of an odd number of neutrons to the $l = 5$, $h_{11/2}$ orbital. This

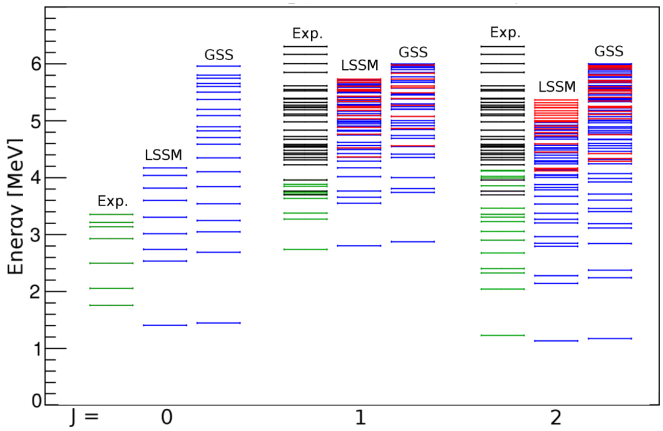

FIG. 10. Experimentally observed energy levels with known spin (green) of $J = 0$, 1, or 2 and unknown spin (black) of $J = 1$ or 2 compared to the *gdsh* shell model and generalized seniority scheme calculations. The blue levels are for the calculated positive parity states, and red levels for the calculated negative parity states. The black levels for $J = 1$ and 2 are identical since these states could be either of these spins.

also supports the lower-energy states in the 3–5 MeV range to be of positive parity, making the case for $J = 2^+$ even more favorable. Based on the branching ratios of these 3–5 MeV levels, shown in Fig. 2, the enhanced ground-state feeding that was observed in Refs. [19,20] is comparable to the present experiment with 13 states having $b_0 \geqslant 0.5$. The threshold of $b_0 \geqslant 0.5$ simply means that the majority of the branching is to the ground state, which is not expected with multiphonon excitations. More states are observed in the region of interest in the present experiment than in the previous PQR studies. However, there is no selectivity in populating states with an isoscalar surface-oscillation compared to the hadronic scattering experiments performed in Refs. [19,20]. Furthermore, the states in the 5–5.5 MeV range show a larger enhancement of the ground-state branching.

Of the 60 excited states placed to the energy region in which the PQR mode is predicted to occur, only seven are assigned as $J = 2^+$. A further 28 of these states could be $J = 2^+$ states based on the direct ground-state decay, but spins $J = 1^+$ or 1^- cannot be excluded for the same reason.

Although there is reason to believe that a large fraction of the states in the 3–5 MeV region are $J = 2^+$, there is great difficulty in assigning a PQR character. Complementary studies to assign spins and parity and which probe low-spin surface excitations would help to identify candidates for the PQR. A firm spin assignment for these newly identified states would also make the comparisons to the theoretical calculations more robust.

Further to identifying states in the 3–5 MeV range, there were several low-energy, 0^+ states observed. A topic of great interest is on $E0$ transitions between states with the same final and initial J value as these are known to be indicative of shape coexistence when an enhanced $E0$ strength is observed. It was possible to indirectly measure the $0_3^+ \rightarrow 0_2^+$ transition by gating on the 7269-keV primary transition as described in Sec. IV. It was assumed that the $0_2^+ \rightarrow 0_1^+$, $E0$ transition of 1758 keV would contribute little intensity to the $0_3^+ \rightarrow 0_2^+$ transition of 299 keV. This is based on the $q_K^2(E0/E2)$ value of 0.236(21) in [32], which is a measure of the intensity ratio of the K-shell component for both the $E0$ and $E2$ transitions: the 1758- and 528-keV transitions, respectively. The present $10^3 \times \rho^2(E0)$ measurement of >38 is in agreement with the previously reported $10^3 \times \rho^2(E0)$ of >36 [32]. It is likely that this value is larger—the lifetime has an upper limit of 200 ps—which would indicate strong mixing between the 0_3^+ state and the 2p-2h, 0_2^+ bandhead.

The 2057-keV, 0_3^+ state has strong mixing with the 2p-2h, 0_2^+ state based on the $\rho^2(E0)$ value in Ref. [32] and the present measured $\rho^2(E0)$ value, and has been suggested to have similar character to the 0_2^+ based on past $E0$ measurements [35]. It is likely that the 0_3^+ and 0_2^+ share some of the 2p-2h character, which could be further explained by the smaller $B(E2; 2_2^+ \rightarrow 0_2^+) = 21(4)$ W.u. observed in ^{118}Sn [10] compared to $B(E2; 2_2^+ \rightarrow 0_2^+) = 44(6)$ W.u. [12] in ^{116}Sn.

While the present $\rho^2(E0)$ value remains a lower limit due to the upper limit of the lifetime for the 2057-keV level, it highlights the possibilities of indirectly measuring $E0$ transitions using γ-ray spectroscopy. Where the capture state is of low spin and positive parity, thermal neutron capture

can be useful in directly populating excited 0^+ states from which primary transitions can be used in γ-γ coincidence gating. Lifetime measurements would be necessary to obtain the $\rho^2(E0)$ values, but it could still be possible to measure the $q_K^2(E0/E2)$ value.

VII. SUMMARY

A high-statistics data set was obtained from the thermal neutron capture reaction, ^{117}Sn(n,γ), performed at ILL, and the results highlight the capabilities of high-precision γ-ray spectroscopy with the FIPPS spectrometer. States at the neutron separation energy (9.326 MeV) in ^{118}Sn were populated and believed to be predominantly 1^+ based on the strong ground-state feedings observed in the γ-ray spectrum. In total, 112 excited states and 567 γ-ray transitions are observed, with 57 levels and 501 transitions being newly observed.

A total of 33 states in the 3–5 MeV region that are assigned as, or could potentially be, 2^+ candidates, decay directly to the ground state. A potential feature of PQR states is that of enhanced branching to the ground state. In the present experiment, 11 states in the 3–5 MeV region have a branching to the ground state $b_0 > 0.4$. Based on LSSM and seniority calculations, it is likely that the majority of these states are $J = 2$. However, it cannot be concluded that PQR states were populated without complementary future studies that specifically probe surface mode excitations which PQR states are believed to be.

The $E0$ transition which connects the 0_3^+, 2057-keV level to the 0_2^+, 1758-keV level was investigated indirectly through γ-γ coincidences. Previously, this $E0$ transition had been observed directly through conversion electron spectroscopy four decades ago [35] around the same time when the lifetime of of the 2057-keV level was measured [36]. The 528-keV transition which decays from the 0_2^+ level was observed through a coincident, primary γ ray that populates the 0_3^+ level. This suggests an unobserved 299-keV, $E0$ transition connecting the 0_3^+ to the 0_2^+. From the measured intensity of the 528-keV transition, it possible to obtain $10^3 \times \rho^2(E0) > 38$ for the 299-keV, $E0$ transition. The branching ratio of the 299-keV, $E0$ transition relative to the $0_3^+ \rightarrow 1230 - keV$, 827-keV, $E2$ transition is 2.5(2)% based on the number of events in the 528-keV, $E2$ transition. Since $E0$ transitions are important to identifying the underlying structure of states with respect to collective and deformed excitations, high-statistics γ-ray data can be a useful tool for indirectly measuring these transitions. Of course, lifetimes are necessary to obtain the transition probabilities. However, compiling a database of branching ratios of $E0/E2$ that can be indirectly determined may simplify the transition probability calculations once lifetimes are measured.

ACKNOWLEDGMENT

This work was supported by the Natural Sciences and Engineering Research Council of Canada (SAPPJ-2023-00025). B.F. Lv would like to thank the National Natural Science Foundation of China (Grant No. 12305128), the Hubert Curien Partnership (PHC) "Cai Yuanpei Project", the International Partnership Program of Chinese Academy of Sciences for Future Network (Grant No. 016GJHZ2023024FN). C. Qi thanks the financial support from the Olle Engkvist foundation and computational resources provided by the National Academic Infrastructure for Supercomputing in Sweden (NAISS) at PDC, KTH.

[1] T. D. Morris, J. Simonis, S. R. Stroberg, C. Stumpf, G. Hagen, J. D. Holt, G. R. Jansen, T. Papenbrock, R. Roth, and A. Schwenk, Phys. Rev. Lett. **120**, 152503 (2018).
[2] T. Togashi, Y. Tsunoda, T. Otsuka, N. Shimizu, and M. Honma, Phys. Rev. Lett. **121**, 062501 (2018).
[3] L. Y. Jia and C. Qi, Phys. Rev. C **94**, 044312 (2016).
[4] K. L. Kratz, B. Pfeiffer, O. Arndt, S. Hennrich, A. Wöhr, the ISOLDE/IS333, t ISOLDE/IS333, and IS393 Collaborations, Eur. Phys. J. A **25**, 633 (2005).
[5] K. L. Jones, A. S. Adekola, D. W. Bardayan, J. C. Blackmon, K. Y. Chae, K. A. Chipps, J. A. Cizewski, L. Erikson, C. Harlin, R. Hatarik, R. Kapler, R. L. Kozub, J. F. Liang, R. Livesay, Z. Ma, B. H. Moazen, C. D. Nesaraja, F. M. Nunes, S. D. Pain, N. P. Patterson *et al.*, Nature (London) **465**, 454 (2010).
[6] S.-S. Zhang, M. S. Smith, G. Arbanas, and R. L. Kozub, Phys. Rev. C **86**, 032802(R) (2012).
[7] R. Dunlop, C. E. Svensson, C. Andreoiu, G. C. Ball, N. Bernier, H. Bidaman, V. Bildstein, M. Bowry, D. S. Cross, I. Dillmann, M. R. Dunlop, F. H. Garcia, A. B. Garnsworthy, P. E. Garrett, G. Hackman, J. Henderson, J. Measures, D. Mücher, B. Olaizola, K. Ortner *et al.*, Phys. Rev. C **99**, 045805 (2019).
[8] K. Whitmore, C. Andreoiu, F. H. Garcia, K. Ortner, J. D. Holt, T. Miyagi, G. C. Ball, N. Bernier, H. Bidaman, V. Bildstein, M. Bowry, D. S. Cross, M. R. Dunlop, R. Dunlop, A. B. Garnsworthy, P. E. Garrett, J. Henderson, J. Measures, B. Olaizola, J. Park *et al.*, Phys. Rev. C **102**, 024327 (2020).
[9] F. H. Garcia, C. Andreoiu, G. C. Ball, N. Bernier, H. Bidaman, V. Bildstein, M. Bowry, D. S. Cross, M. R. Dunlop, R. Dunlop, A. B. Garnsworthy, P. E. Garrett, J. Henderson, J. Measures, B. Olaizola, K. Ortner, J. Park, C. M. Petrache, J. L. Pore, K. Raymond *et al.* (GRIFFIN Collaboration), Phys. Rev. C **103**, 024310 (2021).
[10] K. Ortner, C. Andreoiu, M. Spieker, G. C. Ball, N. Bernier, H. Bidaman, V. Bildstein, M. Bowry, D. S. Cross, M. R. Dunlop, R. Dunlop, F. H. Garcia, A. B. Garnsworthy, P. E. Garrett, J. Henderson, J. Measures, B. Olaizola, J. Park, C. M. Petrache, J. L. Pore *et al.*, Phys. Rev. C **102**, 024323 (2020).
[11] J. L. Pore, D. S. Cross, C. Andreoiu, R. Ashley, G. C. Ball, P. C. Bender, A. S. Chester, A. Diaz Varela, G. A. Demand, R. Dunlop, A. B. Garnsworthy, P. E. Garrett, G. Hackman, B. Hadinia, B. Jigmeddorj, A. T. Laffoley, A. Liblong, R. Kanungo, B. Noakes, C. M. Petrache *et al.*, Eur. Phys. J. A **53**, 27 (2017).
[12] C. M. Petrache, J.-M. Régis, C. Andreoiu, M. Spieker, C. Michelagnoli, P. E. Garrett, A. Astier, E. Dupont, F. Garcia, S. Guo, G. Häfner, J. Jolie, F. Kandzia, V. Karayonchev, Y.-H.

Kim, L. Knafla, U. Köster, B. F. Lv, N. Marginean, C. Mihai *et al.*, Phys. Rev. C **99**, 024303 (2019).
[13] M. Spieker, P. Petkov, E. Litvinova, C. Müller-Gatermann, S. G. Pickstone, S. Prill, P. Scholz, and A. Zilges, Phys. Rev. C **97**, 054319 (2018).
[14] N. Tsoneva and H. Lenske, Phys. Rev. C **77**, 024321 (2008).
[15] H. K. Toft, A. C. Larsen, A. Bürger, M. Guttormsen, A. Görgen, H. T. Nyhus, T. Renstrøm, S. Siem, G. M. Tveten, and A. Voinov, Phys. Rev. C **83**, 044320 (2011).
[16] L. Pellegri, A. Bracco, F. Crespi, S. Leoni, F. Camera, E. Lanza, M. Kmiecik, A. Maj, R. Avigo, G. Benzoni, N. Blasi, C. Boiano, S. Bottoni, S. Brambilla, S. Ceruti, A. Giaz, B. Million, A. Morales, R. Nicolini, V. Vandone *et al.*, Phys. Lett. B **738**, 519 (2014).
[17] D. Savran, M. Babilon, A. M. van den Berg, M. N. Harakeh, J. Hasper, A. Matic, H. J. Wörtche, and A. Zilges, Phys. Rev. Lett. **97**, 172502 (2006).
[18] J. Endres, E. Litvinova, D. Savran, P. A. Butler, M. N. Harakeh, S. Harissopulos, R.-D. Herzberg, R. Krücken, A. Lagoyannis, N. Pietralla, V. Y. Ponomarev, L. Popescu, P. Ring, M. Scheck, K. Sonnabend, V. I. Stoica, H. J. Wörtche, and A. Zilges, Phys. Rev. Lett. **105**, 212503 (2010).
[19] M. Spieker, N. Tsoneva, V. Derya, J. Endres, D. Savran, M. Harakeh, S. Harissopulos, R.-D. Herzberg, A. Lagoyannis, H. Lenske, N. Pietralla, L. Popescu, M. Scheck, F. Schlüter, K. Sonnabend, V. Stoica, H. Wörtche, and A. Zilges, Phys. Lett. B **752**, 102 (2016).
[20] N. Tsoneva, M. Spieker, H. Lenske, and A. Zilges, Nucl. Phys. A **990**, 183 (2019).
[21] C. Petrache *et al.*, Institut Laue-Langevin report (2018), doi:10.5291/ILL-DATA.3-17-20.
[22] C. Michelagnoli, A. Blanc, E. Ruiz-Martinez, A. Chebboubi, H. Faust, E. Froidefond, G. Kessedjian, M. Jentschel, U. Koester, P. Mutti, and G. Simpson, EPJ Web Conf. **193**, 04009 (2018).
[23] S. F. Mughabghab, Thermal neutron capture cross sectionsresonance integrals and G-factors, Brookhaven National Laboratory, upton, NY 11973-5000 (2003).
[24] K. Kitao, Nucl. Data Sheets **75**, 99 (1995).
[25] A. B. Garnsworthy, C. E. Svensson, M. Bowry, R. Dunlop, A. D. MacLean, B. Olaizola, J. K. Smith, F. A. Ali, C. Andreoiu, J. E. Ash, W. H. Ashfield, G. C. Ball, T. Ballast, C. Bartlett, Z. Beadle, P. C. Bender, N. Bernier, S. S. Bhattacharjee, H. Bidaman, V. Bildstein *et al.*, Nucl. Instrum. Methods Phys. Res., Sect. A **918**, 9 (2019).
[26] Y. Loginov, L. M. Smotritskij, and P. A. Sushkov, Bull. Russ. Acad. Sci. Phys. **66**, 1601 (2002).
[27] S. Raman, T. A. Walkiewicz, S. Kahane, E. T. Jurney, J. Sa, Z. Gácsi, J. L. Weil, K. Allaart, G. Bonsignori, and J. F. Shriner, Phys. Rev. C **43**, 521 (1991).
[28] J. R. de Laeter, J. K. Böhlke, P. D. Bièvre, H. Hidaka, H. S. Peiser, K. J. R. Rosman, and P. D. P. Taylor, Pure Appl. Chem. **75**, 683 (2003).
[29] B. Mills and J. Smith, Angular correlation utility bugfixes, dep upgrades (2016), doi:10.5281/zenodo.45587.
[30] J. K. Smith, A. D. MacLean, W. Ashfield, A. Chester, A. B. Garnsworthy, and C. E. Svensson, Nucl. Instrum. Methods Phys. Res., Sect. A **922**, 47 (2019).
[31] P. E. Garrett, M. Zielińska, and E. Clément, Prog. Part. Nucl. Phys. **124**, 103931 (2022).
[32] T. Kibédi, A. Garnsworthy, and J. Wood, Prog. Part. Nucl. Phys. **123**, 103930 (2022).
[33] T. Kibédi, T. W. Burrows, M. B. Trzhaskovskaya, P. M. Davidson, and C. W. Nestor, Jr., Nucl. Instrum. Methods Phys. Res., Sect. A **589**, 202 (2008).
[34] C. Qi and Z. X. Xu, Phys. Rev. C **86**, 044323 (2012).
[35] H. Kawakami, N. Yoshikawa, K. Komura, M. Koike, and H. Yamada, Phys. Rev. C **25**, 2013 (1982).
[36] A. Bäcklin, N. Jonsson, R. Julin, J. Kantele, M. Luontama, A. Passoja, and T. Poikolainen, Nucl. Phys. A **351**, 490 (1981).